DEEPWELL MONITORING OF STRAIN-SENSITIVE PARAMETERS OVER THE GREATER SOUTHERN CALIFORNIA UPLIFT

Thomas L. Henyey, Ta-liang Teng, Douglas E. Hammond, and Charles G. Sammis

Department of Geological Sciences
University of Southern California
Los Angeles, California 90007

USGS CONTRACT NO. 14-08-0001-18383
Supported by the EARTHQUAKE HAZARDS REDUCTION PROGRAM

OPEN-FILE NO. 81-881

U.S. Geological Survey
OPEN FILE REPORT

Twamley

SUMMARY

This final technical report for USGS Contract #14-08-0001-18383 contains the following:

1) A preprint of a paper submitted to Geophysical Research Letters that reports the work on major element chemistry, radon, and seismicity.

2) A preprint of a paper to be published in the Ewing Symposium of JGR on research in acoustic emissions.

3) A status report on the groundwater level - turbidity - thermistor studies along the San Andreas fault.

TABLE OF CONTENTS

PART A

A Search for Co-variance Among Seismicity, Groundwater Chemistry, and Groundwater Radon in Southery California

by

D. E. Hammond
T. L. Teng
G. L. Miller
G. Haraguchi

submitted to

Geophysical Research Letter, February, 1981

ABSTRACT

Several wells and springs near active faults in southern California have been monitored for the concentration of Rn, Na^{+}, K^{+}, Mg^{+2}, and Cl^{-} for periods of up to 24 months, in an effort to see if any of these constituents show variations which may be related to seismic activity. Radon might reflect either a change in the rock surface area to pore volume ratio or a change in groundwater flow characteristics. The chemistry may change with a change in the flow characteristics. Only a few of these sites have shown significant fluctuations in either radon or chemistry. Data from cold springs are consistent with a model in which ionic constituents are controlled by reactions in the soil zone and radon concentrations are controlled by flow rates in the aquifer.

A site in the San Gabriel mountains has shown relatively high radon in the summer and low radon in the winter, apparently following the annual precipitation cycle. However, this site showed no corresponding change in its chemistry. A second site near Wrightwood, California has shown an annual cycle in its chemical composition, but shows no change in radon. Ten days prior to the Big Bear earthquake ($M \sim 4.9$), 65 km to the east, one sample from this site showed a 50% increase in radon, but no change in chemistry. A third site, 20 km north of the Malibu earthquake ($M \sim 5.0$) showed radon variation ranging from 0.4 to 4 times the normal concentration for two months preceding and two months following the event. The chemistry at this site did not change. Within this study area, radon appears to exhibit anomalous variations within several tens of kilometers of impending earthquakes. The mechanism creating these signals has not been elucidated, but does not influence the composition of important ionic constituents. Groundwater radon concentrations may also reflect variations in precipitation but not variations in atmospheric pressure.

INTRODUCTION

Research over the past decade by a number of groups (see King, 1980) has suggested that the radon concentration in groundwater may increase prior to earthquakes, and thus radon may serve as a pre-monitory signal for seismic events. The mechanism (or mechanisms) responsible for such increases has not yet been elucidated, but several factors which may play a role have been discussed by Tanner (1979). One possibility is that dilation of rocks may increase the surface area/pore volume of rocks near the source area, resulting in increased radon emanation per unit volume of pore fluid. A second possibility is that groundwater flow patterns and flow rates may be influenced by either fracturing or strain accumulation. Changes in the flow field might also result in changes in water chemistry as waters from different horizons mix. In addition to stress related changes, environmental phenomena such as rainfall, temperature, and atmospheric pressure fluctuations may introduce variability in groundwater radon concentrations. With these possibilities in mind, we have monitored the major element chemistry and radon concentration in several wells and springs in southern California.

METHODS AND SITE DESCRIPTION

Thirteen sites have been monitored for radon over periods from two to seven years (figure 1). These sites were selected for their proximity to major faults, coverage of a wide geographic area, and suitability of sampling. Duplicate radon samples are collected by volunteers in the field and either mailed or hand carried to the laboratory. Sample bottles are one liter aluminum bottles fitted with inlet and outlet tubes. Bottles are filled either by evacuating the container and drawing water with the vacuum or by slowly filling an unevacuated bottle through a tube inserted to the bottom of the bottle.

Radon is measured in the laboratory by circulating helium through the sample and then a glass trap immersed in liquid nitrogen. After extraction

is completed, the trap is isolated from the sample and warmed, water and acidic gases are removed on drierite and ascarite, and the sample is transferred to a leucite cell containing a thin coating of ZnS phosphor which is sensitive to alpha decay. Scintillations from radon and two alpha emitting daughters are counted with a photomultiplier until the statistical uncertainty in counting is 1%. Appropriate decay corrections are made. The efficiency of the counting cells is determined by extracting standard solutions of radium-226. The precision of efficiency determination is about ± 3%, and the precision of duplicate samples is about ± 5%. The water remaining after radon extraction is stored in acid-cleaned glass bottles for later analysis of cations and anions.

Four of the radon sites were selected for time-series cation and anion analysis, on the basis of the behavior of radon and the location of the sample site. Chloride was measured coulometrically with an automatic titrator. Precision is ± 1% or ± 0.02 mM, whichever is larger. Hot spring waters with H_2S showed some interference, which could be removed by aerating an acidified sample. Sodium and potassium were measured by atomic absorption spectrometry, and magnesium and calcium were measured by atomic absorption spectrometry or by EDTA titrations if the concentrations were large. Duplicate analyses had a precision of ± 2%. Calcium showed considerable variability in time series analyses, probably due to $CaCO_3$ precipitation during radon analyses, and these data are of little value. Potassium data will not be presented here since the variations were essentially the same as those observed for sodium. Blanks for the glass storage bottles were monitored, and were only significant for very dilute samples (corrections are always 10% of the total).

Rainfall data were taken from precipitation stations as close as possible to the well sites. Seismic data were taken from the SCARLET array data reports (Hutten et al., 1978; 1979).

SITE DESCRIPTIONS

ARP Well (AR) - located at the base of the San Gabriels in sandy soil probably underlain by crystalline rock. Samples are taken weekly from a wellhead which is pumped by the Metropolitan Water District.

Arrowhead Springs (AS) - located in the San Bernardino Mountains in an area underlain by crystalline rock. Samples are taken every 2-4 weeks (later weekly) from a pipe which taps a hot spring (T = 74°C).

Big Pines (BP) - located in the San Bernardino Mountains, within 1 km of the San Andreas fault zone, in an area of sandy soil which is probably underlain by crystalline rock. Samples are drawn weekly from the wellhead of a pump which periodically supplies water for the Big Pines campground in the Angeles National Forest. A spring lies approximately 60 m (vertical drop) downslope from the site. This spring flows all year round, although the flow rate varies.

Seminole Hot Springs (SH) - located in the Santa Monica Mountains in sandy soil, probably underlain by sedimentary rocks. A pump discharges warm (T = 39°C) water into a pool. Bubbles are sometimes observed in the pump effluent. Samples are drawn weekly from the outlet jet of the pump.

RESULTS AND DISCUSSION

Data from these sites are shown in figures 2-5, along with pertinent environmental variables. Seismic events are also indicated by arrows on these plots. The likelihood of strain accumulation influencing any site will depend on a number of geological and hydrological factors. The probability of observing a radon anomaly prior to an earthquake might be proportional to the strain energy released and inversely proportional to the area over which strain energy is accumulated. Directional factors may also be important, but are difficult to evaluate. In order to illustrate seismicity in the study area and to qualitatively index the likelihood of observing a radon anomaly, a function expressing this

relationship can be calculated:

$$P = A \frac{\exp (3.4\ M)}{R^2}$$

where M = earthquake magnitude

R = separation of monitoring sites and epicenter (km)

A = a normalization factor (chosen to be 10^{-3} for convenience)

This probability index was chosen so that it increases by a factor of 30 for each unit of magnitude increase. This function was then calculated for all earthquakes (M > 3.5) in the study area. The largest value observed was at Seminole Hot Springs where P = 60 for the Malibu earthquake (1-1-79 M = 5.0). At the sites studied in detail only two values of P > 10 were observed and six values of P > 1 were observed. These are indicated by arrows in figures 2-5. Epicentral locations are indicated in figure 1.

Results of time series analyses at the ARP well are shown in figure 2. Radon at this site shows a close relationship to rainfall. When it rains, radon concentrations are low and when it is dry, radon concentrations are high. This suggests that groundwater is diluted by fresh rainfall, but analysis of ionic constituents over one of these cycles shows no evidence of dilution. An alternative explanation is that the concentrations of ionic species are controlled by processes in a soil zone. Radon concentrations primarily reflect the history of aquifer waters for the week prior to sample collection. If the equilibrium concentration of radon is low in a zone where ionic constituents are acquired and the residence time is long, and if the equilibrium radon concentration is high in an aquifer zone where the residence time is short and variable, the observed data for this site are easily explained. High rainfall results in a short aquifer residence time and low radon concentrations. This data suggests that radon can vary in response to groundwater flow rates.

The Big Pines site (figure 3) also shows a response to rainfall. At this site, however, concentrations of ionic constituents decrease in response to

rainfall, but radon shows no change. All ionic constituents decrease several months after the onset of winter rains, and then increase during dry months. All elements show phase lags relative to rainfall. Chloride responds most quickly and shows the largest fractional changes, while magnesium and sodium show longer phase lags and smaller fractional variations. The phase lag in time is smaller in 1978, when rainfall was greater, than in 1979. These observations suggest that at this site, the residence time of water in the soil zone, where ionic constituents are acquired, is short (several months) and variable. Cation concentrations are buffered by ion exchange processes and chloride is not well buffered. However, the residence time of water in the flowing aquifer is sufficiently long during all seasons that no change in radon is observed. This site was 70 km from the Big Bear earthquake (6-30-79, M = 4.9, P = 3.5). A small radon anomaly was observed in the sample collected 8 days prior to the event. Another sample was collected one day prior to this event, but was delayed for 4 weeks in the mail. This data (not plotted) also suggested high radon concentrations, but the low levels of radon remaining when the sample was received and the uncertainties in blanks preclude definite conclusions about the radon behavior prior to the event.

Data from the Arrowhead Springs site (figure 4) shows one large fluctuation in December, 1978. This sample shows concentrations or radon and ionic constituents which are only 40% of normal. Apparently this sample was diluted, but how this dilution occurred is not clear. This site was closer to the Big Bear earthquake (30 km), but no unusual radon behavior was clearly observed. A number of reports have indicated correlations between emission of soil radon and atmospheric pressure. It is unlikely that such a correlation exists between groundwater radon concentrations and atmospheric pressure. A regression analysis between atmospheric pressure (three day average) and radon concentration at each site showed that no correlation exists, as expected. It should also be

noted that the sampling interval is 3-4 weeks at this site and short-lived spikes in radon concentrations could be missed. Craig et al. (1980) observed large increases in radon, helium, methane, argon, and nitrogen at a site near this one about 60 days prior to this event.

Data from the Seminole Hot Springs site is plotted in figure 5. Eleven months of radon data prior to the period plotted showed fairly uniform concentrations, ave. ($\pm 1\sigma$) = 1008±237. Large fluctuations were observed after October, 1978. Values ranging from 0.5 to 4 times the average were observed prior to and following the Malibu earthquake (1-1-79, M = 5.0, P = 60). Ionic constituents showed no fluctuations (note expanded scales) during this period. The cause of the radon fluctuations is not obvious, although it could be related to strain accumulation. It is possible that different sources of water were reaching the surface, although the constancy of ionic constituents makes this an unlikely explanation. Fluctuations could be caused by variations in the transit time to the surface from zones adding large amounts of radon to these thermal waters. Fluctuations could also be caused by collecting samples containing variable amounts of gas bubbles. Duplicate samples showing the large increases only agreed within 25%, which is far above the normal precision. Poreda et al. (1978) have demonstrated the presence of additional gases associated with high radon concentration in thermal springs. However, variations in the total gas content are not likely to produce the low concentrations of radon observed at this site, unless samples collected prior to October 1978 had a very constant fraction of gas phase collected with the water sample (about 15% by volume) and samples collected from mid-November, 1978 to mid-January, 1979 had almost no gas phase collected. Fluctuations could also be caused by microfracturing of rocks, producing fluctuations in the rate of radon emanation from rocks. At present it is not possible to distinguish which, if any, of these mechanisms caused the radon fluctuations.

CONCLUSIONS

In summary, the following conclusions may be inferred from our data.

1) Radon concentrations in cold springs of shallow origin can respond to temporal precipitation patterns, apparently due to changes in aquifer flow rates. Ionic constituents need not show any response.

2) Ionic constituents of groundwater may show changes in response to precipitation, apparently due to changes in the residence time of water in the soil zone. These changes need not be accompanied by changes in radon concentrations.

3) Anomalous radon behavior was observed in a thermal spring prior to and following the Malibu earthquake. Analysis of seismic activity in proximity to sampling sites indicates that this site is the one most likely to show anomalous behavior. No variations in the concentrations of ionic constituents was observed, suggesting that the mechanism causing this radon variation event is probably not mixing of different groundwaters. Alternatively, the radon variation may be due to a change in the transit time from a region of high radon concentration to the surface.

ACKNOWLEDGEMENTS

The assistance of R. McElrath, D. Green (for ARP), J. Pilcher (for Arrowhead), E. Shumann (for Big Pines), and C. Stamm (for Seminole Hot Springs) in collecting water samples in the field and Ming Huang in the laboratory analysis has been appreciated. This research has been supported by U. S. Geological Survey contracts #14-08-0001-16745, -18383, and -15875.

REFERENCES

Craig, H., Y. Chung, R. Poreda, J. Lupton, S. Damesceno, Fluid phase earthquake precursor studies in southern California, Trans. Am. Geophys. Union, 61, p. 1035, 1980.

King, C.-Y., Geochemical measurements pertinent to earthquake prediction, J. Geophys. Res., 85, p. 3051, 1980.

Poreda, R., Y. Chung, J. Lupton, R. Horowitz, and H. Craig, Investigation of radon and helium as possible fluid phase precursors to earthquakes, Trans. Am. Geophys. Union, 59, p. 1196-97, 1978.

Tanner, A. B., Radon migration in the ground: a supplementary review, U.S.G.S. Open-file Report 78-1050, 1978.

FIGURE CAPTIONS

Figure 1. Index map of southern California wells and springs with long-term radon records are located by triangles and identified by code letters. Stations discussed in detail are solid triangles. The epicenters of significant earthquakes occurring within the monitoring period are also shown. Dashed lines trace the San Andreas fault (SA), San Jacinto fault (SJ), Garlock fault (GA) and San Gabriel fault (SG).

Figure 2. Radon, sodium, chloride, and rainfall vs. time at the ARP well (AR). Radon concentrations show the monthly averages ($\pm 1\sigma$) of 3-5 samples. Rainfall is the monthly total at a station in Pasadena.

Figure 3. Radon, magnesium, sodium, chloride, and rainfall vs. time at Big Pines (BP). Rainfall is the monthly total at the Big Pines Forest Service Station. Arrows indicate dates of nearby earthquakes. P is an index to evaluate the likelihood of observing an earthquake precursor and is discussed in the text.

Figure 4. Radon, sodium, and chloride vs. time at Arrowhead Springs (AS). Arrows indicate dates of nearby earthquakes. P is an index to evaluate the likelihood of observing an earthquake precursor and is discussed in the text.

Figure 5. Radon, sodium, and chloride vs. time at Seminole Hot Springs (AH). Arrows indicate dates of nearby earthquakes. P is an index to evaluate the likelihood of observing an earthquake precursor and is discussed in the text.

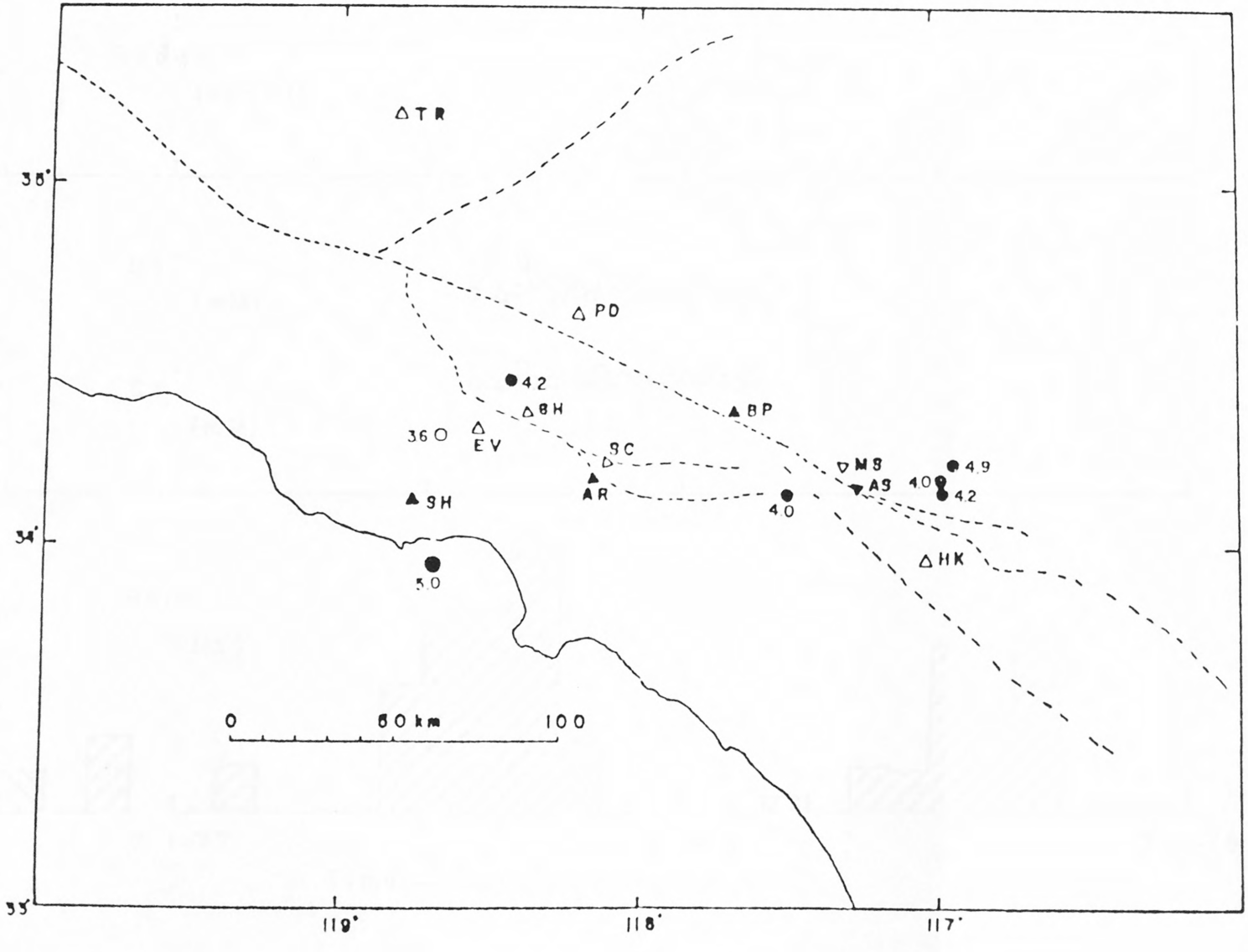
△TR
△PD
●42
△BH
360
△EV
▲BP
△SC
▲AR
▽MS
▼AS
●49
40
●42
●40
▲SH
●50
△HK
0
50 km
100
36°
34°
33°
119°
118°
117°

Fig. 1

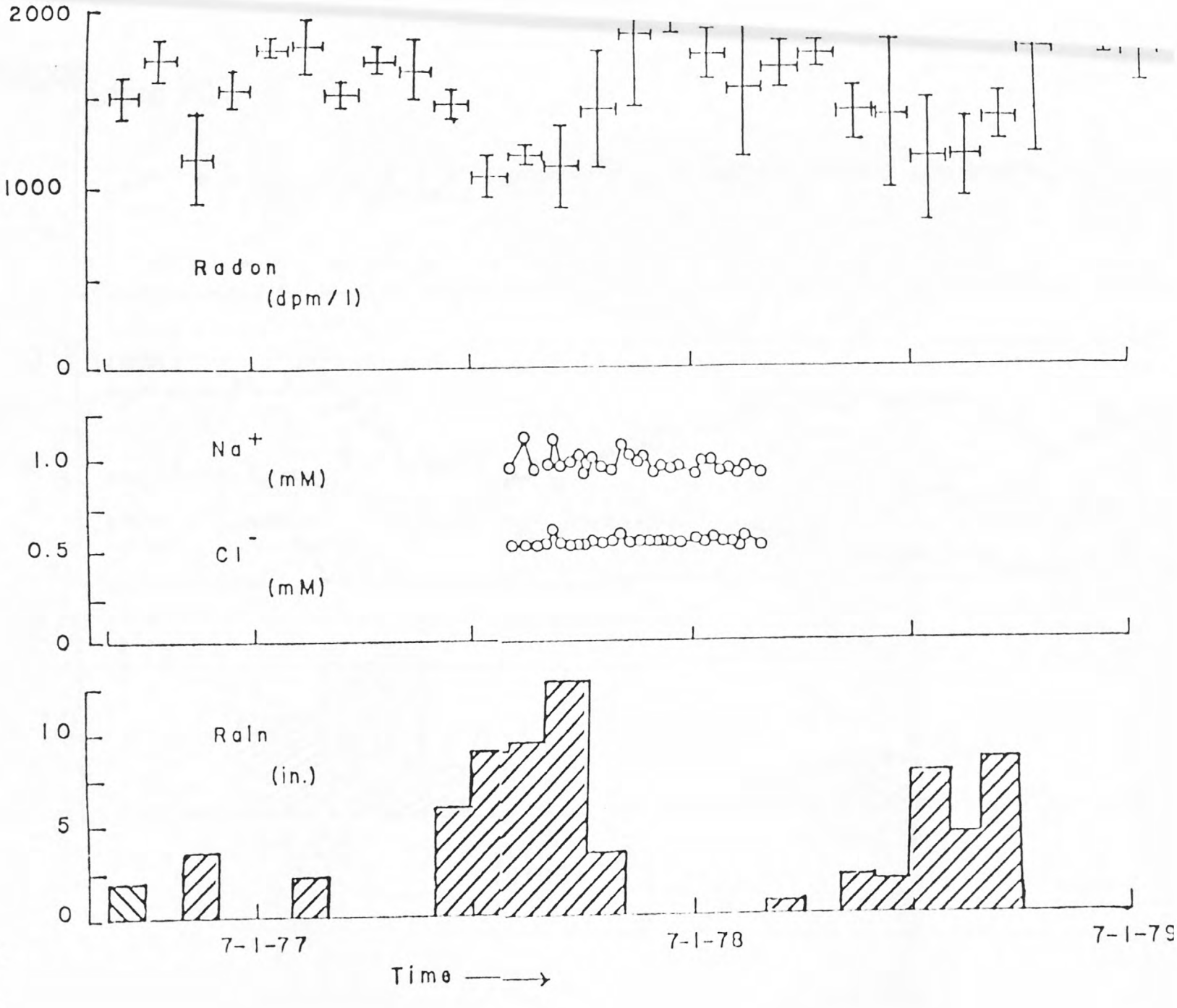
2000
1000
0
Radon
(dpm / l)
1.0
0.5
0
Na+
(mM)
Cl-
(mM)
10
5
0
Rain
(in.)
7-1-77
7-1-78
7-1-79
Time

Fig. 2

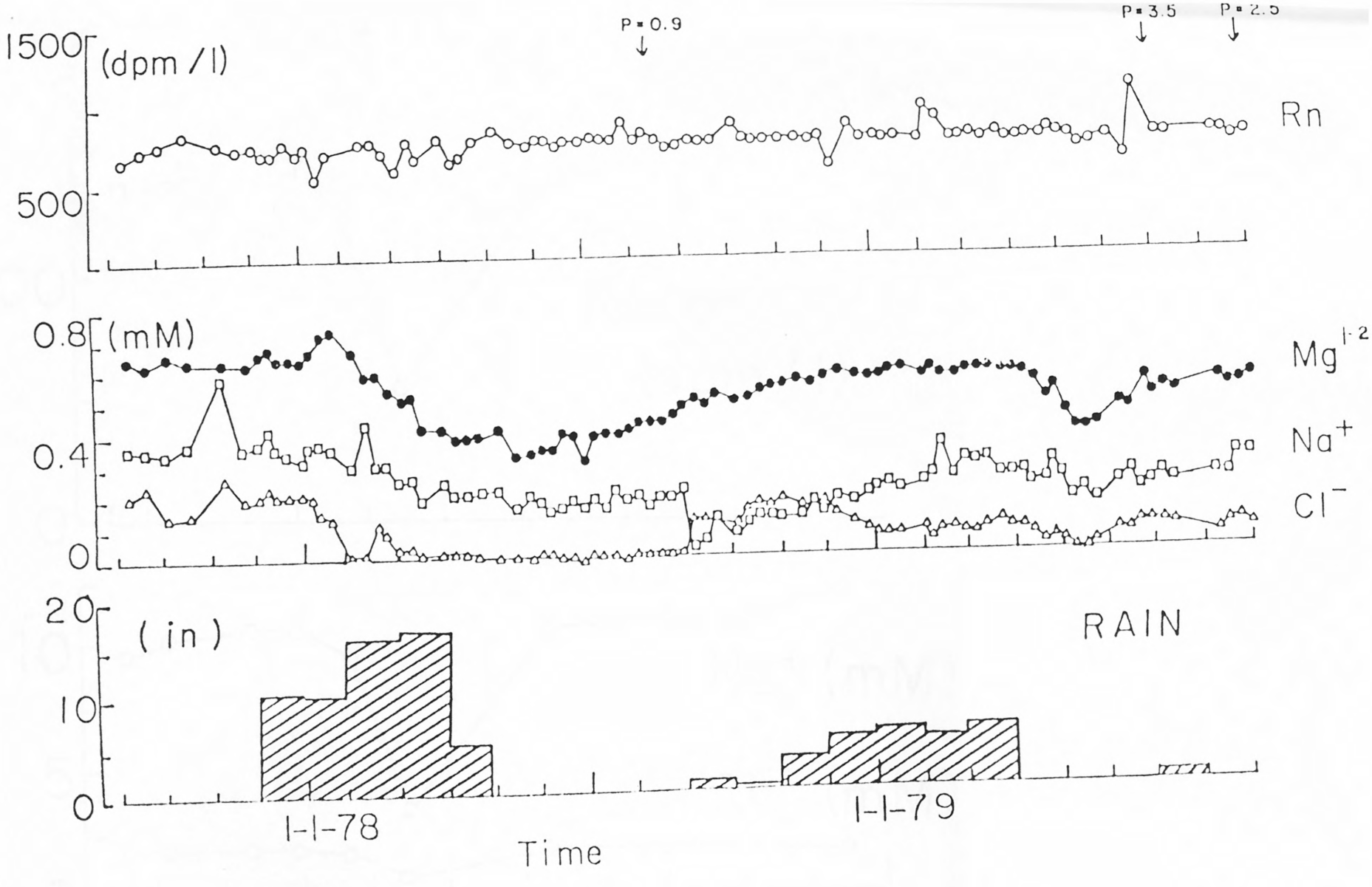
P = 0.9
P = 3.5
P = 2.5
1500
(dpm / l)
500
Rn
0.8
(mM)
0.4
0
Mg 1·2
Na+
Cl−
20
(in)
10
0
RAIN
1-1-78
1-1-79
Time

Fig. 3

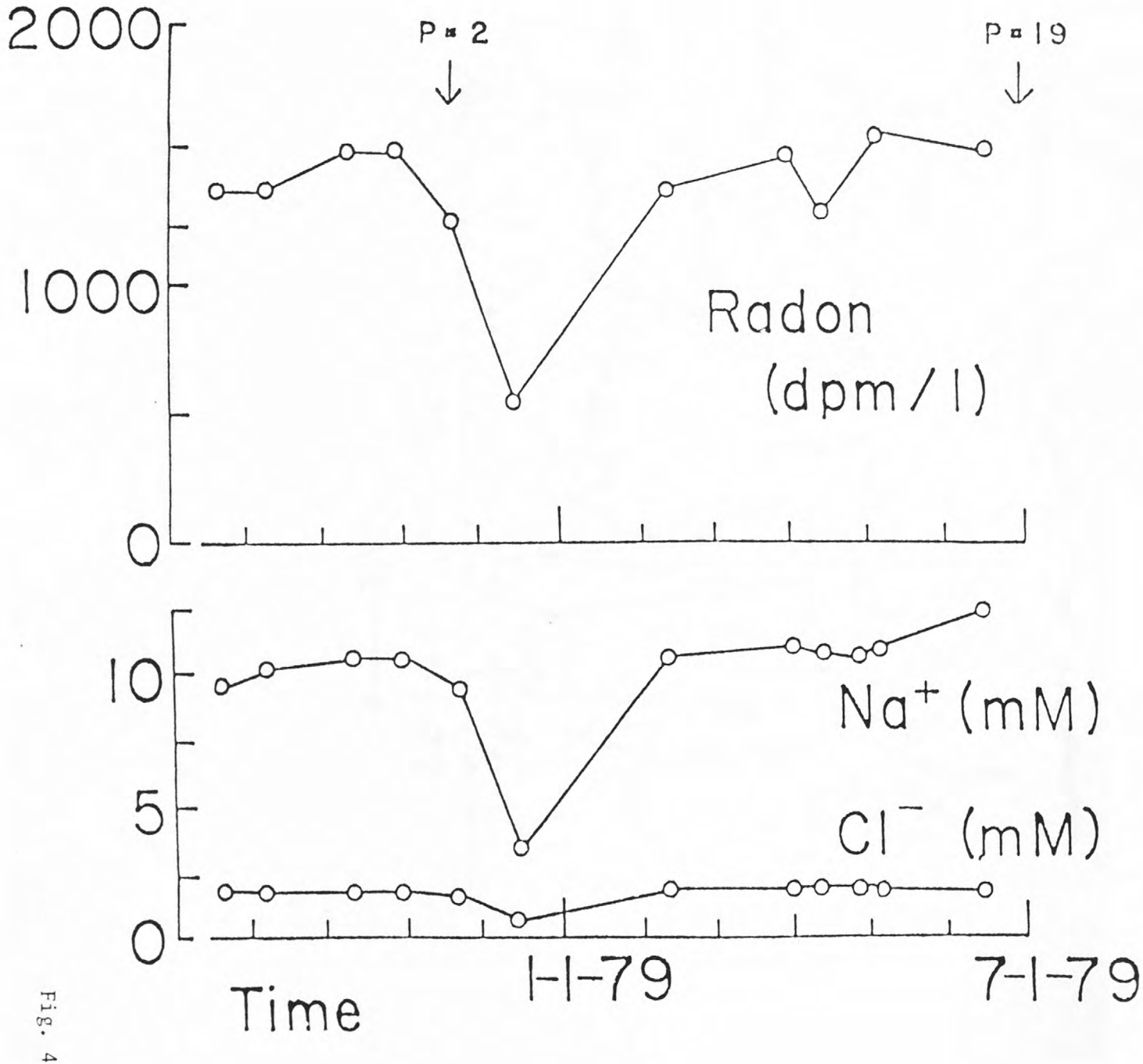

Fig. 4

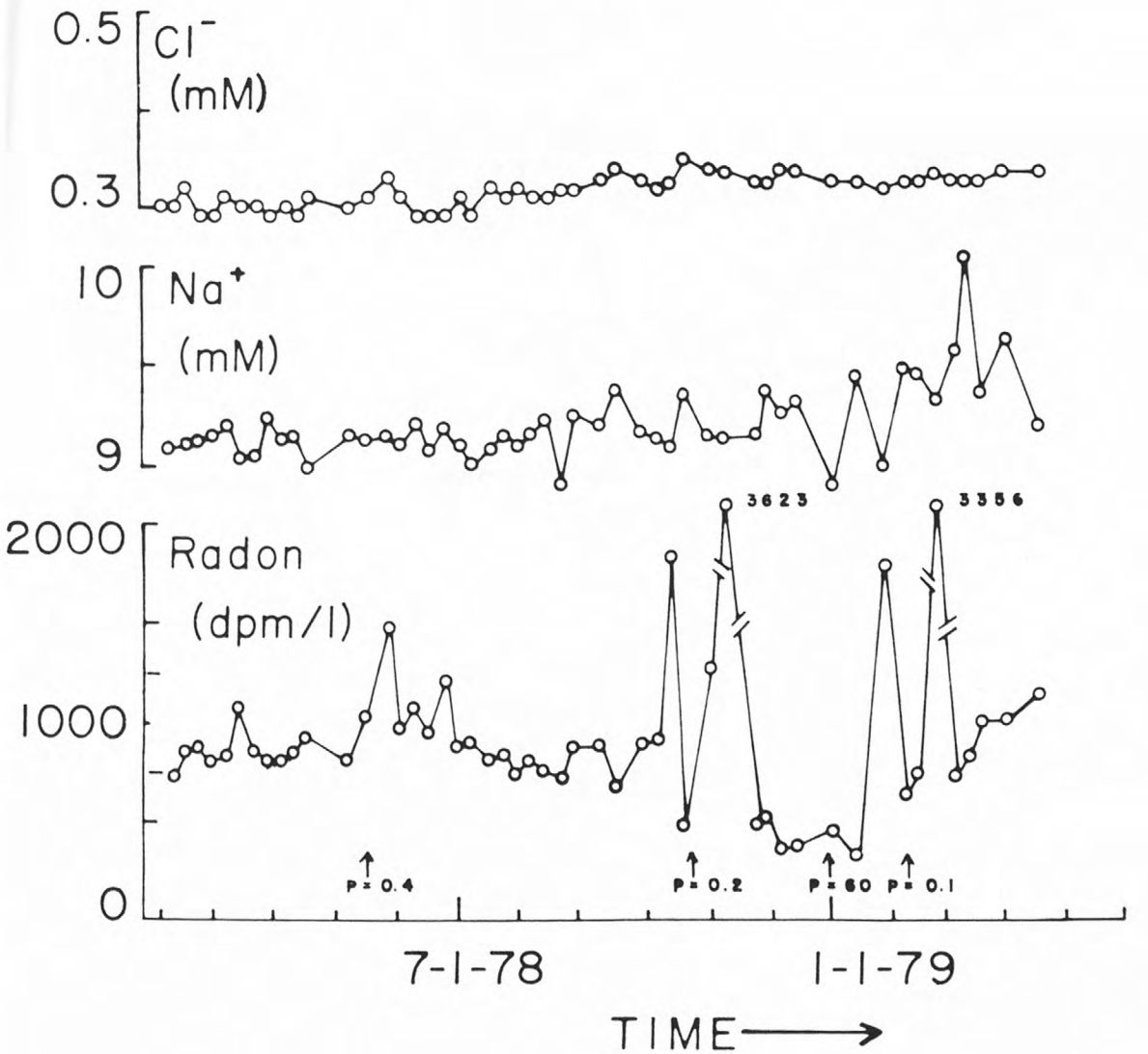
0.5
Cl⁻
(mM)
0.3
10
Na⁺
(mM)
9
2000
Radon
(dpm/l)
1000
0
3623
3356
P = 0.4
P = 0.2
P = 60
P = 0.1
7-1-78
1-1-79
TIME

Fig. 5

PART B

The Detection of Nanoearthquakes

by

Ta-liang Teng
Thomas L. Henyey

to be published in

Ewing Volume, J.G.R.

THE DETECTION OF NANOEARTHQUAKES

Ta-liang Teng and Thomas L. Henyey

Department of Geological Sciences, University of Southern California
Los Angeles, California 90007

Abstract. High-frequency, wideband (20 Hz to 16 kHz) recording instruments for the detection of minute seismic emissions in borehole environments have been designed, developed, and deployed in three deep wells within seismically active regions. Two of these well sites are within a few km of the San Andreas fault near Palmdale, California; the third site is at the Monticello Reservoir, South Carolina. Seismicity near the Monticello Reservoir is induced by the recent impounding of water. The sensor is a highly-sensitive hydrophone emplaced at the bottom of the fluid-filled well. The surface recording package is an analog event recorder complete with event-detecting logic and digital delay circuit. At all three sites, numerous minute seismic emissions were detected with dominant spectral energy in the band 0.5 to 5 kHz and a peak at about 2 kHz. These events have durations of the order of 10 to 100 milliseconds and waveforms similar to a near-field earthquake greatly scaled down in size. Risking downward extrapolation of the duration time vs. magnitude relationship, these events may be assigned magnitudes in the range of -1 to -5; as such we call them nano-earthquakes. With their high-frequency content and in view of the strong attenuation in the upper crust, these nanoearthquakes are probably occurring at distances less than one km from the sensor. If laboratory results are applicable to field situations, the frequency of occurrence of nanoearthquakes may reflect the state of ambient stress, and their rate of occurrence may be useful in identifying the approximate time when a large earthquake is imminent.

Introduction

Minute elastic radiation is known to occur in a stressed rock. Repeated observations in the laboratory and in the field (mainly coalfields) show that these emissions begin to occur as the applied stress reaches a certain threshold characteristic of the rock medium. The frequency

of occurrence increases rapidly as the stress increases. As time progresses, the sources of these emissions tend to converge toward a location where the final rupture usually would take place. This pre-rupture elastic radiation process would be very attractive in light of possible application to the prediction of natural earthquakes.

Much has been reported on pre-earthquake anomalous animal behavior; some of these animals are noted for their hearing sensitivity. Reports of audible sounds before the occurrence of large earthquakes are also common. Although many of these reports lack scientific credibility, especially after-the-fact narrations, some of them appear to be valid observations and cannot be easily dismissed. Davison (1938) has compiled descriptions of sounds accompanying or preceding earthquakes; he concludes that 58 to 72 percent of the sounds occurred before earthquakes. Lawson (1908) also reports sounds before the 1906 San Francisco earthquake and its aftershocks. The report of earthquake sounds before shocks in China dates back to 474 A.D. A partial compilation of these reports is given in Table 1. Reports after 1968 are generally obtained through group observations that cannot be explained by individual illusions. The descriptions of earthquake sounds in this table are very similar; they are also similar to those given by Davison (1938) and others (see, for example, Wallace and Teng, 1980). Of particular interest in these reports is a probable rough correlation of earthquake magnitude with precursory time. For large earthquakes ($M > 6\ 1/2$), precursory times from hours to days are reported. Such phenomena, if shown to be real, may furnish a very desirable precursory signal for imminent earthquake predictions.

Hill et al. (1976) conclude that under favorable conditions acoustic waves can be excited by seismic P and SV waves impinging at the earth's surface. However, this seismic-to-acoustic excitation is not an efficient process and earthquake sounds are likely to be perceptible only in the immediate neighborhood of seismic disturbances. Calculations by Hill et al. (1976) suggest that it is much more efficient to study minute seismic emissions by placing sensors in the earth rather than to attempt microphone pickups of seismically-induced earthquake sounds or acoustic emissions. This paper discusses our work on instrument design, and the detection and analysis of seismic excitations recorded by hydrophones in deep water-filled boreholes.

There is ample experimental evidence leading to the present field study. In the laboratory, deformation experiments of brittle rocks are accompanied by emissions of elastic energy which Mogi (1962 a, b; 1968) called elastic shocks, and Scholz (1968 a, b, c) referred to as microfractures. Studies of these events have led to an improved physical understanding of the failure mechanism that is the most probable underlying cause of earthquake occurrence (Lockner and Byerlee, 1977; Weeks, Lockner and Byerlee, 1978; Dieterich, 1978; and Kranz, 1980). There is a close similarity between laboratory deformations of brittle rocks and deformation of the crust. Both generate events that follow a similar frequency-magnitude distribution. One can define a continuous spectrum of elastic excitations from 10^{-3} Hz to almost 1 MHz that would accommodate the wave phenomena of large earthquakes (10^{-3} - 10^{0} Hz), microearthquakes (10^{0} - 10^{2} Hz), landslides ($\sim 10^{2}$ Hz, Cadman and Goodman, 1967), rock bursts (10^{2} - 10^{3} Hz, Antsyferov, 1966), and laboratory rock fracturing experiments of varying scales (10^{5} - 10^{6} Hz). Assuming a typical velocity of 4 km/sec for crustal rocks, we find that laboratory fracturing of brittle rocks produces elastic waves with wavelengths in the range of 4 cm to 4 mm, corresponding to microfracturing across grain boundaries, or boundaries between small heterogeneities. For rock bursts with wavelengths in the range 40 m to 4 m, one cannot invoke a grain boundary dislocation mechanism. Crustal irregularities of larger dimensions (large cracks, joints, etc.) are necessary to explain the generation of these excitations.

Rock bursts have been intensively studied (see volumes edited by Antsyferov, 1966; and Hardy and Leighton, 1977). Using a recording system with flat response from 10 to 500 Hz, McGarr and Green (1978) recorded numerous micro-tremors during aftershock sequences to several M=1 to M=1.5 events in a deep mine. Application of a high-frequency seismological method to geomechanics problems, particularly associated with mining operations in coalfields, has led to successful prediction of rock bursts, which bear close resemblance to scaled-down natural earthquakes. It is regularly observed that, prior to rock bursts, an anomalous increase in the number of minute seismic emissions first takes place. However, an anomalous occurrence of this seismic radiation is not found to be a sufficient condition for a subsequent rock burst; such an occurrence may correspond to a natural earthquake swarm as a scaled-up counterpart.

With these background experimental results, we speculate that in a stressed rock body of 10 - 100 km in dimensions, there may exist a continuous radiation of minute seismic events, the activity level of which serves as one manifestation of the ambient stress state. To differentiate these field events from those observed in the laboratory, and from microearthquakes which have much lower frequency spectra and much higher energy content, we call them nanoearthquakes. Nanoearthquakes have magnitudes of less than -1, and are the natural downward continuation of microearthquakes. Nanoearthquakes may have a more-or-less homogeneous distribution over the entire volume of the stressed rock body, that is, a volume with dimensions substantially larger than those of the eventual rupture surface. This postulated homogeneous occurrence of nanoearthquakes may correspond to Mogi's (1968) stage B in a laboratory experiment. As the ambient stress increases and it enters Mogi's stage C, two conditions could exist: (1) If the field observation sites were in close proximity to the eventual rupture surface, one might observe a continuing increase in the level of occurrence of these nanoearthquakes. This increase would become more rapid as the rupture is approached; and (2) If the field observation sites were at some distance ($\sim$ 10 - 100 km) from the eventual rupture surface, Mogi's stage C would be accompanied by a gradual decrease in the activity level before the eventual rupture. Unless coverage of an earthquake prone area was extensive, case (2) would be more likely. For such observations to be of practical use, we would first need to know if these nanoearthquakes are numerous enough to be analyzed statistically, and second what the time duration of the field equivalent of Mogi's stage C is likely to be. Considering the data in Table 1, this duration may be of the order of hours to days for large ($M > 6\ 1/2$) earthquakes, which may be sufficiently long for purposes of earthquake prediction. To test these hypotheses, we have designed and constructed appropriate field equipment, and have deployed the equipment in deep boreholes drilled into rock bodies known to have been under ambient stress loading. A discussion of our experimental work follows.

Instrumentation

A high-frequency seismic event recording system suitable for field deployment was designed and

constructed to detect and study the possible occurrence of nanoearthquakes in stressed rocks. The entire system consists of a downhole sensor, a downhole preamplifier, and a surface event recorder with a time code generator and regulated power supply. A cable up to several thousand feet long connects the downhole instruments with the surface recorder. This cable carries power to supply the downhole preamplifier and transmits the signal from the downhole sensor to the surface recording package. The sensor is a broadband (1 Hz to 100 kHz) hydrophone with a sensitivity of 1 volt/μbar. One stage of preamplifier with 40 db gain is applied to the signal next to the sensor and used as a line driver for the long cable.

In situ recording is necessary since the expected signals contain frequencies too high for telephone telemetry. However, in the future, rather than relying on waveform analysis and recording the entire waveform, the recording system can be greatly simplified to merely an event counter. Thus its output becomes a low sample rate signal (in terms of number of events per hour) which can be brought back to the laboratory through a variety of telemetry devices.

Figure 1 illustrates a block diagram of the recording system, which is a broad-band analog event recorder normally operated in a standby mode. A 60 db gain amplifier is placed at the front end. When an input signal amplitude exceeds a preset level, an event detector circuit triggers and initiates a fast-start instrument-quality analog tape recorder which runs at a speed of 3 - 3/4 ips and delivers a frequency response up to 16 kHz. A signal delay system has been introduced to avoid the loss of signal during the initial 400 ms start-up of the tape recorder. It consists of an A/D converter with 8 bits parallel output. Each parallel bit is followed by an array of 20 shift register chips with 1024 bits per chip. With a 40 kHz clock drive, a total signal delay of 512 ms is realized. The recombined delayed signal is passed through a D/A converter and a low-pass filter to remove any noise higher than 16 kHz. The signal is then recorded on one track of the tape recorder. Since the low-frequency cutoff of the tape recorder is about 20 Hz, the overall system has a bandwidth of 20 Hz to 16 kHz.

Parallel to the input signal is the timing signal generated by a crystal clock. Since the input signal is expected to be short in duration

(a fraction of a second), the after-event duration has been set to be 10 sec. to conserve the recording tape. A special circuit has been constructed to generate a 10 sec. time frame. This consists of a digital clock, calendar circuit, and its accompanying display and the time code generator circuit. In each ten-second period, time of day is displayed once every second for eight seconds, and the month and date once every four seconds. A Ni-Cd rechargeable battery is used to power the clock to prevent loss of clock information due to power failure. The entire recording system is packaged in a 26" x 20" x 16" fiberglass case for field deployment (Figure 2).

Field Studies

Field sites were prepared parallel to instrument development. Downhole deployment is necessary to avoid surface noise (Bacon, 1975). Deep boreholes of sufficiently large diameter are used for emplacement of the sensor-preamplifier package. Three field sites have been used to date. In southern California, two abandoned wildcat oil wells near the San Andreas fault in the Palmdale area were selected. The Skelton well (34°30'N, 118°14'W) was drilled entirely in granitic rock 3 km NE of the San Andreas fault. This well has 10 3/4" surface casing for the first 65 m and is uncased 8 3/4" hole to an accessible depth of 300 m. The Del Sur well (34°39'N, 118°14'W) was drilled in Tertiary/Quaternary sandstones and shales 6 km NE of the San Andreas fault. The well is cased with 6 5/8" casing to a total depth of 700 m. A third field site, the "Monticello #2" well (34°18'N, 81°19'W) was drilled by the U.S. Geological Survey for experiments related to microearthquake activity induced by the impounding of water in Monticello Reservoir. Precise hypocenter locations show the seismicity to be in clusters at depths up to about one km (Talwani, 1979). The well was drilled to a depth of 1 km into granite/gneiss and is uncased except near the surface.

In each case, the hydrophone-preamplifier package was lowered by winch to the well bottom. Sufficient cable was fed into the well to allow for total relaxation of the cable. AC power was connected to the regulated power supply of the surface recording system through an isolation transformer to prevent spurious power line noises from being introduced into the recording circuit. After the sensor was properly emplaced, a few hours were allowed for the sensor to equilibrate with the ambient environment. The recorder gain was adjusted for the maximum sensitivity permitted by the background noise. Data gathered from the three field deployments are discussed below.

Data Analysis and Discussion

A large number of nanoearthquakes were recorded during the three separate field deployments described above. For illustration, a number of these events are reproduced in Figures 3 and 4. These are typical of events from the Skelton and the Monticello wells.

Recordings from the Skelton and Monticello wells were subjected to waveform analysis. At this stage of our experimental work, we seek to answer two questions: 1. Is high-frequency seismic radiation generated in stressed rocks in the field? And if so, 2. What is the character of its waveforms? The existence of numerous events such as those in Figures 3 and 4 indicates the answer to the first question to be affirmative. To study the waveforms, the analog recording tapes were played back through a fast sample-and-hold device and in turn the digitized data were fed through a minicomputer which stored the digitized events on disk. At a sampling rate of 40 kHz, the playback system was consistent with the bandwidth of the recording system. Signals on the disks were dumped one file at a time back through the minicomputer and displayed on an oscilloscope. Signals were carefully examined, and windowed for spectral analysis. Figures 3 and 4 give, respectively, some typical unclipped nanoearthquake waveforms and their corresponding spectra. Since photographs were taken from the oscilloscope, some of the signal tails were omitted although the accompanying spectrums were obtained for the entire waveforms. Durations of the nanoearthquakes are primarily in the range of 5 to 100 ms. The unclipped amplitude is of the order of 10 μbar. Risking the downward extrapolation of the total duration vs. magnitude scale (Real and Teng, 1973), the corresponding magnitudes for these events are -1.5 to -4 (using an equation by McGarr and Green, 1978, the magnitude range is -2 to -5). From the spectra, one finds the dominant energy peak to be about 2 kHz. This peak drops off sharply at the low-frequency end. The data from the Skelton well show little or no energy below 1.5 kHz, whereas the Monticello data have energy down to 1 kHz and below. The high-frequency end does not drop off as sharply; occasional secondary peaks are present. Little energy exists beyond 6 kHz. It is interesting to note that the nanoearthquakes have very similar waveforms and spectrums whether from the Skelton well in California or from the Monticello well in South Carolina. Since the sensor is a

hydrophone emersed in the borehole fluid, no shear waves were recorded; the converted compressional waves from incident shear waves at the rock-fluid interface were probably small, and no such phase was identifiable. Assuming the S-P interval velocity to be ∿ 10 km/sec (or 10 m/ms) and that shear-converted compressional waves are not negligible in amplitude, the maximum epicentral distance of these nanoearthquake sources should not exceed 1 km. For a signal duration of 10 ms, the source distance probably is less than 100 m. The playback data also show that these nanoearthquakes occur rather sporadically in groups.

During the recording period, at least 30 events per day were recorded at the Skelton well and about 500 at the Monticello well. For these two periods of recording, instruments were set at comparable gain. If all other ambient conditions are the same, a high event rate would suggest a high stress state (Mogi, 1968; Lockner and Byerlee, 1977). Recent results from hydro-fracturing stress measurements at sites near Palmdale and at the Monticello well site also suggest that the Monticello well is subject to a higher ambient stress (Zoback, 1980). For a given monitoring site, if the number of nanoearthquakes detectable is large enough to make the time series statistically meaningful, then the rate of nanoearthquake occurrence may be used as a reference for the ambient stress state, and thus as an earthquake precursory parameter. The short detection distance (<< 1 km) is not a severe drawback, so long as during stress buildup (e.g. Mogi's stage B), the occurrence of nanoearthquakes is more-or-less homogeneous over the entire source region. This region may have dimensions on the order of 10-100 km, depending on the magnitude of the impending earthquake. Thus, for a given monitoring site away from the eventual rupture surface, first a gradual increase of the event rate of nanoearthquakes may be observed, followed by a short quiescent period before the final rupture.

At the Del Sur well, recorded signals had much higher frequency content. The waveforms also show a characteristic pulse shape that is not expected from a typical disturbance of seismic origin. We suspect that these signals may be related to the casing-wall rock interaction since the Del Sur well is cased over its entire length. The Del Sur recorder also captured the M=5.3 Santa Barbara earthquake of August 13, 1978, and many of its aftershocks (Figure 5). The epicenter of the Santa Barbara earthquake was ∿ 120 km W of the recording site. Much of the high-frequency (>> 20 Hz) content of the seismic waves was lost

along the relatively long travel path, and frequencies lower than 20 Hz were not well recorded by the band-limited tape recorder. Nevertheless, the events were still large enough to be recorded due to the high gain setting, and the onsets of signal arrivals were preserved.

Our findings are quite preliminary. Further confirmation on the seismic origin of these detected signals must be carefully established. This work suggests that future nanoearthquake detection or monitoring should be performed in uncased wells. Better identification of the source distance would be desirable. A waveform recorder as described in this paper is important for the first phase of the project, during which characterization of nanoearthquakes and their sources are of prime importance, especially to establish whether they originate from rock failures. If so, for the next phase of practical application, the complex recorder can be replaced by an event counter that produces low sampling rate data of perhaps one datum point (in terms of number of events) per minute or per hour as compared to a 16 kHz sampling rate for the current instrument. The simplification of recording instruments would make widespread applications practical and the low data rate would make on line monitoring through telemetry methods possible.

Acknowledgments

We would like to thank Liang-Fang Sun for his instrumentation and field deployment work. John McRaney and Derek Manov assisted in various phases of the field work. Advice and cooperation from Barry Raleigh, Mark Zoback, and Pradeep Talwani were instrumental in the results from the Monticello well of South Carolina. This research was funded by U.S. Geological Survey contracts 14-08-0001-16613 and -16745.

References

Antsyferov, M.S., Principals of the application of seismo-acoustics to coal seams subject to rock bursts, in Seismo-Acoustic Methods in Mining, ed. by M.S. Antsyferov, Consultants Bureau, New York, pp. 1-8, 1966.

Armstrong, B.H., Acoustic emission prior to rockbursts and earthquakes, Bull. Seismol. Soc. Am., 59, no. 3, pp. 1259-1279, 1969.

Bacon, C.F., Acoustic emission along the San Andreas fault in southern central California, Calif. Geol., 28, pp. 147-154, 1975.

Byerlee, J.D., and P. Lockner, Acoustic emission during fluid injection into rock, proceedings of the first conference on acoustic emission in geologic structures and materials, Trans. Tech Publications, Claustal, W. Germany, 1977.

Cadman, J.D. and R.E. Goodman, Landslide noise, Science, 158, pp. 1182-1184, 1967.

Davison, C., Earthquake sounds, Bull. Seismol. Soc. Am., 28, pp. 147-161, 1938.

Dieterich, J.H., Preseismic fault slip and earthquake prediction, J. Geophys. Res., 83, no. B8, pp. 3940-3949, 1978.

Hardy, H.R. Jr., and F.W. Leighton, ed: Proceedings first conference on acoustic emissions/ microseismic activity in geologic structures and materials, Trans. Tech Publications, Clausthal, Germany.

Hill, D.P., F.G. Fischer, K.M. Lahr, and J.M. Coakley, Earthquake sounds generated by body-wave ground motion, Bull. Seismol. Soc. Am., 66, no. 4, pp. 1159-1172, 1976.

Kranz, R.L., The effects of confining pressure and stress difference on static fatigue of granite, J. Geophys. Res., 85, no. B4, pp. 1854-1866, 1980.

Lee, T.Y., and X.K. Hu, A preliminary study on the relationship between earthquake and earthquake sound, Acta Geophysica Sinica, 23, no. 1, pp. 94-101, 1980.

Lockner, D., and J. Byerlee, Acoustic emission and creep in rock at high confining pressure and differential stress, Bull. Seismol. Soc. Am., 67, pp. 247-258, 1977.

Lockner, D., A. Lindh, and J. Byerlee, Apparent velocity anomalies and their dependence on amplitude (abstract), E.O.S. Trans. Am. Geophys. Union, 58, p. 433, 1977.

Lawson, C.A., The California earthquake of April 18, 1906, Report of State Earthquake Investigation Commission, VI, Carnegie Institution of Washington, 1980.

McGarr, A., and R.W.E. Green, Microtremor sequences and tilting in a deep mine, Bull. Seismol. Soc. Am., 68, no. 6, pp. 1679-1697, 1978.

Mogi, K., Study of elastic shocks caused by the fracture of heterogeneous materials and its relation to earthquake phenomena, Bull. Earthquake Res. Inst., 40, pp. 125-173, 1962a.

Mogi, K., Magnitude-frequency relation for elastic shocks accompanying fractures of various materials and some related problems in earthquakes, 2, Bull. Earthquake Res. Inst., 40, 831-853, 1962b.

Mogi, K., Source locations of elastic shocks in the fracturing process in rocks, Bull. Earthquake Res. Inst., 46, pp. 1103-1125, 1968.

Pao, Y.H., Theory of acoustic emission, elastic waves and non-destructive testing of materials, AMD - 29, ed. Y.H. Pao. The American Society of Mechanical Engineers, New York, pp. 107-128, 1978.

Real, C.R., and T.L. Teng, Local Richter magnitude and total signal duration in southern California, Bull. Seismol. Soc. Am., 63, No. 5, pp. 1809-1827, 1973.

Scholz, C.H., Microfracturing and the inelastic deformation of rock in compression, Geophys. Res., 73, no. 4, pp. 1417-1432, 1968a.

Scholz, C.H., Experimental study of the fracturing process in brittle rock, Geophys. Res., 13, no. 4, pp. 1447-1454, 1968b.

Scholz, C.H., The frequency-magnitude relation of microfracturing in rock and its relation to earthquakes, Bull. Seismol. Soc. Am., 58, no. 1, pp. 399-415, 1968c.

Talwani, P., Induced seismicity, earthquake prediction and crustal structure studies in South Carolina, Summaries of Technical Reports, VIII, National Earthquake Hazard Reduction Program, U.S.G.S., 1979.

Weeks, J., D. Lockner, and J. Byerlee, Changes in b - values during movement on cut surfaces in granite, Bull. Seismol. Soc. Am., 68, pp. 333-341, 1978.

Wallace, R.E., and T.L. Teng, Prediction of the Sungpan-Pingwu earthquakes of August 16, 1976, Bull. Seismol. Soc. Am., 70, no. 4, pp. 1199-1224, 1980.

Zoback, M., Personal Communication, 1980.

TABLE 1a. Earthquake Sound Reports from Historical Documents

ntral a	Date	M	Precursory Time	Description	Notes
;i	7/474	4-5	Minutes	Sounded like thunder a dozen times, earthquake followed.	A, p. 184
ning	10/24/1594	4-5	Minutes	In the morning, a rumbling of distant thunder approached from NW. As it came close, windows rattled. Shortly after, buildings started shaking.	A, p. 322
ndon	7/25/1668	8.5	One day	The day before the main shock, the rumbling sound of a rushing river was heard.	A, p. 636
;oning	12/11/1855	5-6	Minutes to Hours	Before the quake, a roll of thunder was heard that alarmed people to go outdoors.	A, p. 339
chuan	9/12/1850	7	One hour	Shortly after lunch, a burst of sound suddenly came from the NW, about an hour later river overflow and strong ground motions followed.	A, p. 1210

otes: A. The historical earthquake data of China, two volumes (in chinese, compiled by Academia Sinica, 1973).

TABLE 1b. Earthquake Sound Reports from Mass Observations

central rea	Date	M	Precursory Time	Description	Notes
ndong	4/02/68	5.2	One Minute	Sounded like a peal of thunder, or the passing of a tractor.	B
andong	7/26/69	6.4	Two Days	Divers reported sound heard below water.	C
n-nan	1/05/70	7 3/4	One Day	A rumbling sound came from the mountains.	D
handong	8/10/70	5	Minutes to Hours	Before the quake, it sounded like thunder, strong wind, a train going over a bridge, or a jet airplane.	E
Yun-nan	5/29/76	7.6	Minutes to half an hour	Rumbling thunder, passing tanks or tractors heard up to a distance of 80 km, over extensive surrounding areas. Sound came from consistent direction when heard from large distance, appeared non-directional when heard very near the epicenter.	F
Sichuan	8/16/76	7.2	An hour to half a month	Sounds of an airplane, single bursts of frog croaking, and long rolls of a thunder were heard at different times and locations.	G

Notes:

B. Shandong earthquake brigade, 1969, a brief report on the Quan Hsien, Shandon and Da Ming, Hebei earthquake of April 2, 1968 (in Chinese). PRC State Seismological Bureau Report.

C. Yangjiang earthquake investigation team for Macroscopic Phenomena, 1969, investigation report, PRC State Seismological Bureau Report.

D. State Seismological Bureau of People's Republic of China, 1970, a macroscopic investigation on the seismo-geological phenomena of the Tunghai, Yunnan earthquake of January 5, 1970, PRC State Seismological Bureau Report.

E. Shandon Earthquake Research Center, 1970, a survey report on Qu-pu earthquake, Appendix I, PRC State Seismological Bureau Report.

F. Chen, L.D., and Chao, W.C., 1979, Lungling earthquake of 1976, a compilation of observations, Earthquake Publishing Company, Beijing, China.

G. Sichuan Provincial Seismological Bureau, 1979, Sungpan earthquake of 1976, a compilation of observations, Earthquake Publishing Company, Beijing, China.

Figure Captions

ure 1. A schematic diagram of the high-frequency event recorder.

Figure 2. The complete high-frequency event recorder system (minus downhole cable). In the center is an instrument quality analog tape recorder with fast start (400 ms). To its right are the detection and digital delay circuits, plus a crystal clock. The box to its left is a regulated power supply. The cylinder at the bottom is the downhole preamplifier; the sensor hydrophone is in the middle of the small coil of cable.

Figure 3. Some typical nanoearthquake waveforms as recorded by a pressure transducer (left) and their corresponding spectrums (right) recorded at the 300 m deep bottom of the Skelton well near Palmdale, California. The well is 3 km from the San Andreas fault.

Figure 4. Some typical nanoearthquake waveforms as recorded by a pressure transducer (left) and their corresponding spectrums (right) recorded at the 1 km deep bottom of the Monticello #2 well in the immediate vicinity of the Monticello dam in South Carolina. The impounding of the reservoir has induced numerous seismic swarm activities. These swarms have focal depths up to about 1 km, and into the swarm hypocenter clusters are the Monticello wells drilled by the USGS.

Figure 5. Recording of the Santa Barbara earthquake of August 13, 1978 and its aftershocks.

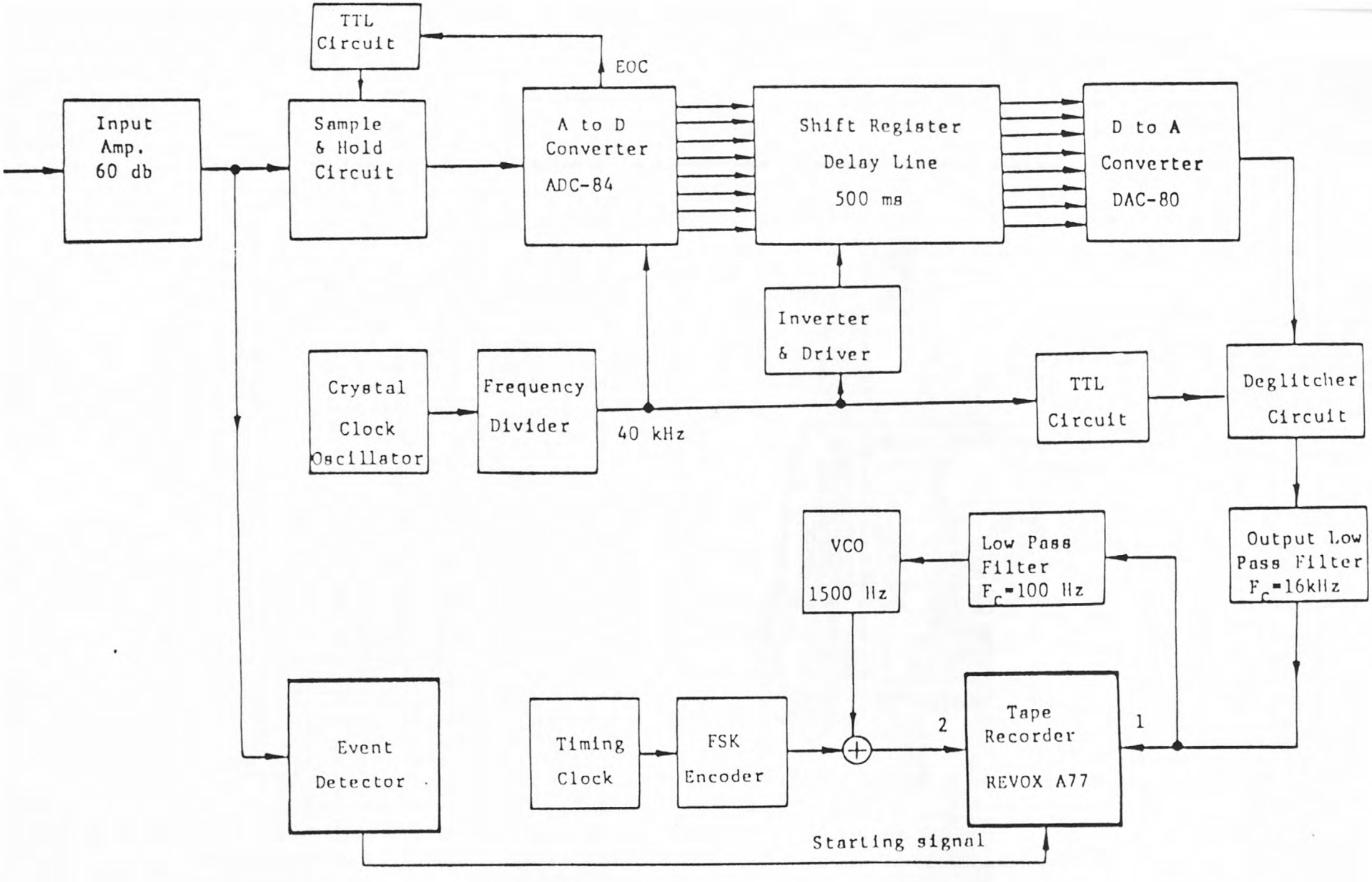
TTL Circuit
EOC
Input Amp. 60 db
Sample & Hold Circuit
A to D Converter ADC-84
Shift Register Delay Line 500 ms
D to A Converter DAC-80
Inverter & Driver
Crystal Clock Oscillator
Frequency Divider
40 kHz
TTL Circuit
Deglitcher Circuit
VCO 1500 Hz
Low Pass Filter F_c=100 Hz
Output Low Pass Filter F_c=16kHz
Event Detector
Timing Clock
FSK Encoder
2
Tape Recorder REVOX A77
1
Starting signal

Fig. 1

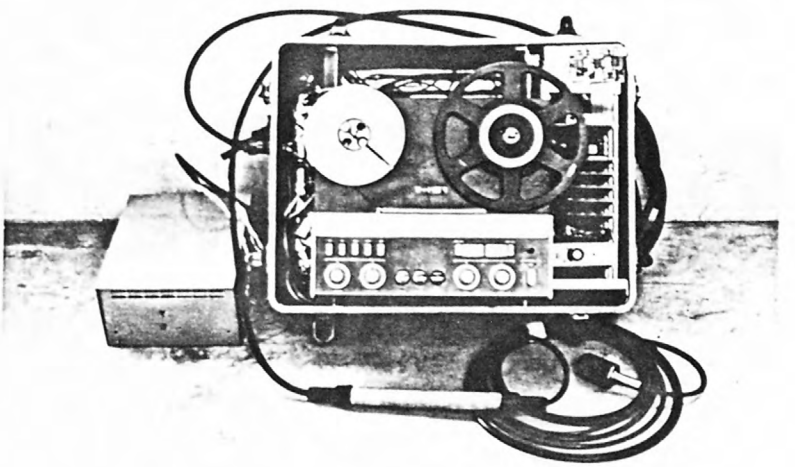

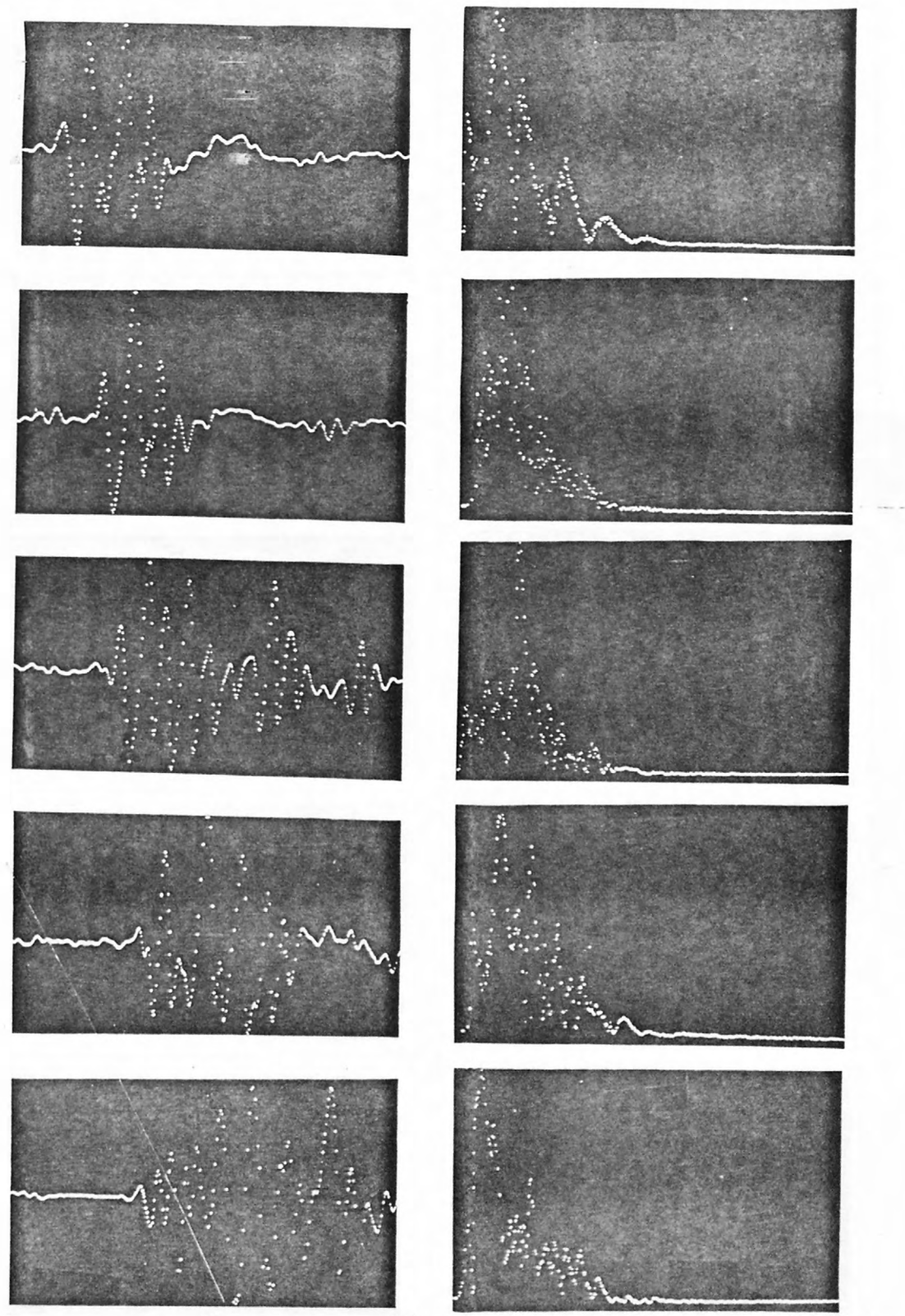

NANOEARTHQUAKES

Fig. 3

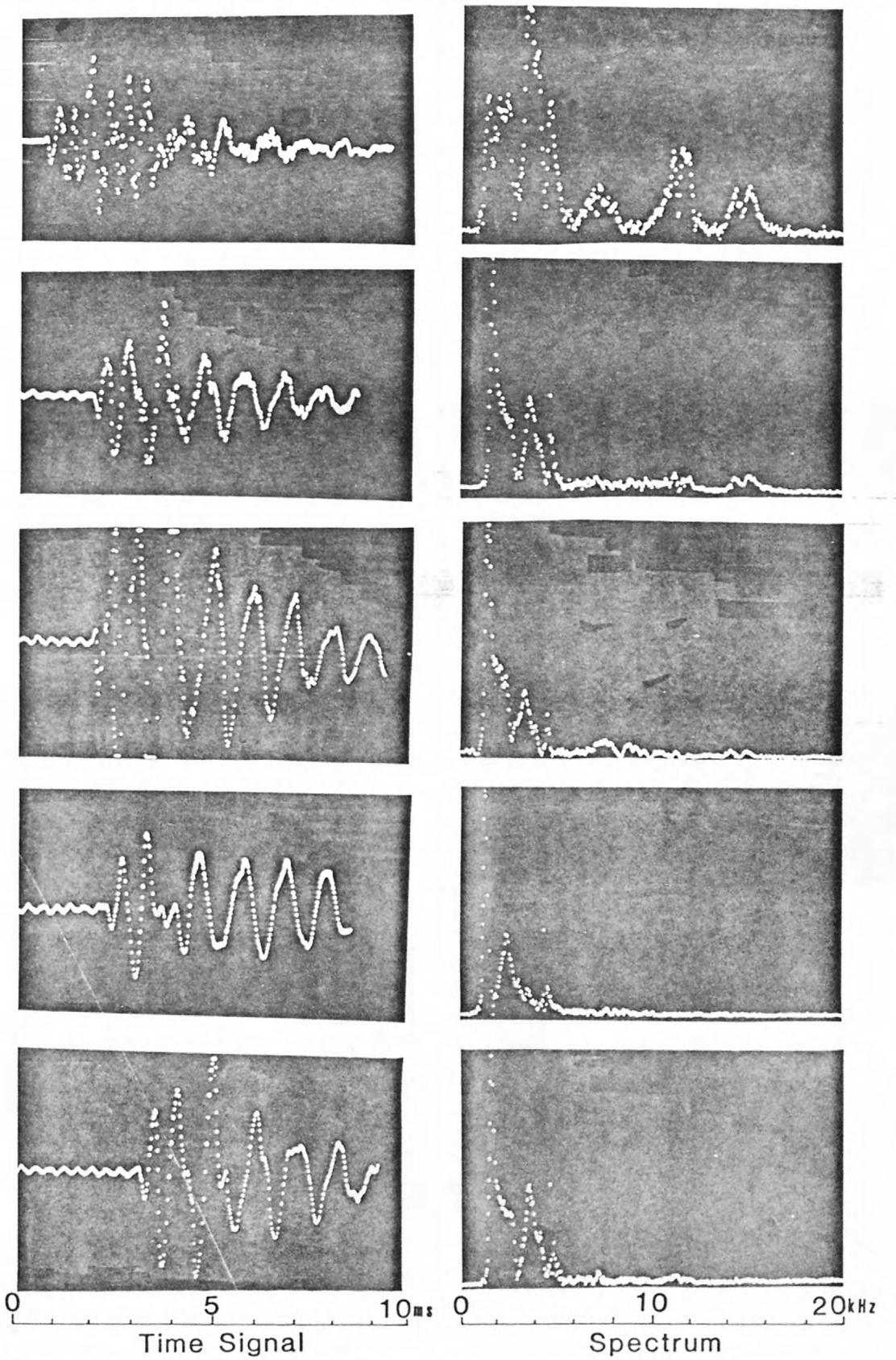

NANOEARTHQUAKES

Fig. 4

A. Santa Barbara Mainshock, August 13, 1978

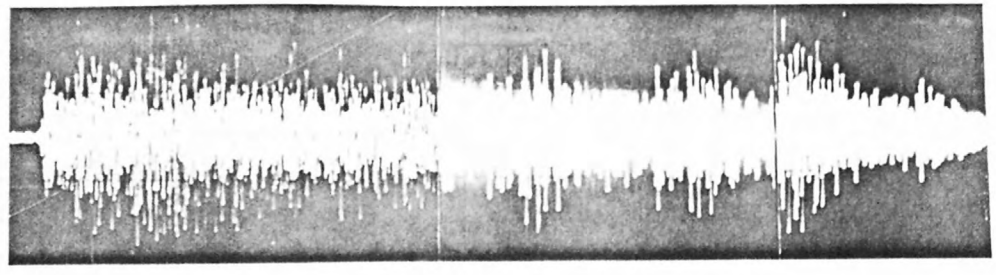

10 s

B. Aftershocks

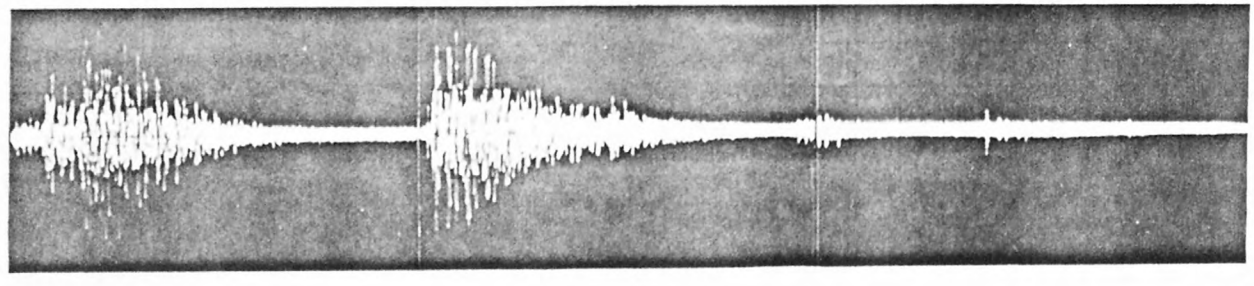

10 s

C. An Enlarged Portion of A

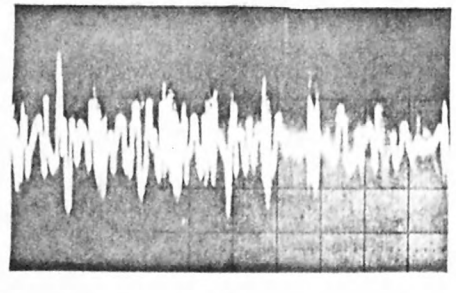

1 s

Fig. 5

PART C

Status Report on Water Level-Turbidimer-Thermistor Package

I. INTRODUCTION

Reports of changes in groundwater levels, flow rates, chemistry and even turbidity preceding and during large seismic events are widespread in the earthquake literature. Pre-seismic strains acting on groundwater basins or aquifers near major faults clearly cannot be ruled out, even though regional dilatancy may in fact not exist. Although aquifer flow rates are relatively slow, the pressure response in large aquifers, such as exist in the western Mojave region, should be considerably faster. This is borne out by observations of earth tide-generated water level changes in wells (Melchior, 1956; Bredehoeft, 1967; Bodvarsson, 1970; Johnson et al., 1973). In such cases, appreciable flow is not required for changes of millimeters to a few feet in the apparent water tables.

Relatively rapid pressure fluctuations will trigger not only water level changes, but also can be expected to induce small changes in the local thermal regime and may free trapped interstitial gases and particulate matter, thereby increasing turbidity. The search for strain/groundwater induced thermal changes in wells is appealing due to (a) the high sensitivity of modern temperature sensors (thermistors), and (b) the fact that surface generated thermal noise is rapidly attenuated in the earth; temperatures at depths of even a few hundred meters have been found to be stable to better than 0.01°C over periods of years by persons reoccupying holes for heat flow measurements.

Over the past few years, we have reclaimed a set of abandoned wildcat oil wells in the western Mojave Block in which to monitor groundwater variations. The wells are located (figure 1) in a variety of geologic terrane and range in depth from 500' to 5500' (see table 1); they were selected from a much larger well population after extensive investigations and work-over operations by commercial rigs. Security and environmental housings have been placed at most well-heads, and in some cases, AC power and telemetry lines installed. These deep holes represent a major scientific investment and must be preserved and used; many sample a large

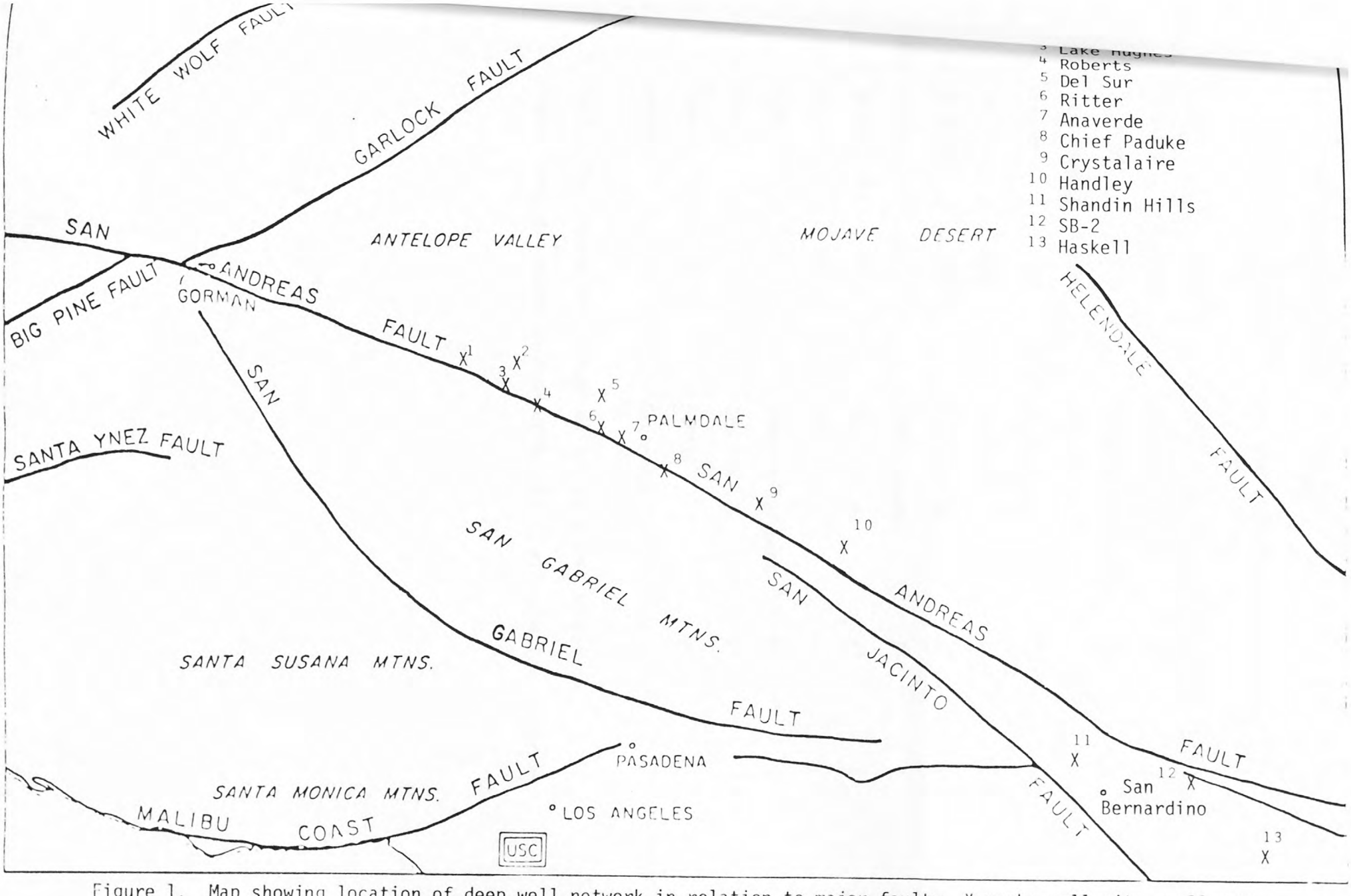

Figure 1. Map showing location of deep well network in relation to major faults. X marks well site, well names in upper right correspond to numbers at well sites.

TABLE 1

Deep Well Sites and Instrument Deployment

Site	Depth	Rock Type	Water Level	Turbidity	Thermistor
Skelton	2200'	Granite	X[1]	X	X
Fairmont	650'	Granite-Sediments	X[1]	X	X
Lake Hughes	1250'	Granite			X
Roberts	550'	Fault Gouge	X[1]	X	
Del Sur	2300'	Sediments	X[1]	X	X
Anaverde	900'	Fault Gouge	X[2]	X	X
Ritter	500'	Fault Gouge	X[1]	X	X
Chief Paduke	1100'	Fault Gouge	X[2]	X	X
Crystalaire	2800'	Granite	X[1]	X	X
Handley	5500'	Granite-Sediment	X[1]	X	X
SB-2	2300'	Granite	X[2]		
Shandin Hills	800'	Schist	X[2]		
Haskell	3300'	Sediments		X	X

[1]water level measurements made using Digiquartz transducer.

[2]water level measurements made using old strain-gage type instrument.

section of the near-surface hydrologic regime.

We have developed a set of water level, turbidity and temperature sensors for use in these wells. Development has emphasized

1) deployment in deep as opposed to shallow wells;

2) compatibility with multiple sensors down-hole;

3) long term down-hole service;

4) high resolution and low drift.

Approximately 50% of our instrumentation is now in place (table 2), with the remaining 50% scheduled for emplacement during the current fiscal year. Funds are requested to maintain the equipment and provide for data collection, handling and analysis.

II. INSTRUMENTATION

Instruments consist of (1) a commercially available quartz oscillator pressure transducer, (2) an optical transmissometer (turbidimeter) based upon a commercial design and built at U.S.C., and (3) a U.S.C. designed and fabricated thermal sensor/gradiometer. Sensors are interfaced to a digital cassette datalogger with time base. Instrumental development has been agonizingly slow due to numerous problems which include:

a) cable breakdown (we are now using cables with integrally molded end connectors and bulkhead feedthrough of the central strain member);

b) pressure sensor drift and deterioration;

c) insensitivity of early turbidimeter;

d) faulty datalogger design;

e) cross-talk between multiple sensors down-hole.

The current generation of sensors and their electronics, discussed below, have solved most of these earlier problems.

A. Water Level

We had originally hoped to sense water level using strain-gage type pressure transducers. However, the units we selected experienced excessive drift and occasional breakdown. As such, we purchased seven quartz oscillator pressure transducers from Digiquartz. These units have a practical resolution of $\sim$ 0.5 mm of H_2O and sense differentially, thus permitting suppression of the superposed atmospheric pressure. They show exceedingly good long term stability and reliability. It was necessary to design, build and field test frequency to analog converters for interfacing the transducers to our dataloggers. We are presently operating these units at 5 mm resolution.

B. Turbidity

The basic design of our turbidimeter has been discussed in earlier U.S.C. technical reports to the U.S.G.S. (e.g. Henyey et al., 1977, 1978). The optical block consists of two phototransistors and two incandescent light bulbs in a diamond shaped array. Four partially independent light paths result, thereby permitting cancellation of changes in output due to source/sensor aging and clouding of the optical windows. The devices have an output range of 2 volts (totally clear water to virtually opaque water). Absolute calibrations have not been run, nor have the response curves been determined, although good sensitivity to low level turbidity has been observed in the lab. Only relative turbidity is presently being monitored. Relatively sophisticated (and still somewhat temperamental) electronics are necessary to cycle the light sources, synchronize and amplify the outputs, and perform the analog ratio and logarithmic computations necessary to achieve a final output voltage proportional to turbidity. We anticipate considerable more work during the current fiscal year in refining the turbidimeter electronics as well as our understanding of the sensor itself.

C. Temperature

The temperature probe consists of two well calibrated thermistors separated by 0.5 m. Thus both absolute temperature and temperature gradients can be monitored. Both thermistors together with known precision resistors are

connected in series at the surface; a constant current source is applied to the network and voltages across each element are cyclically sensed using the same bridge/amplifier network.

D. Data Recording and Playback

Datel dataloggers together with control networks are used to record in the field at a rate of 6 samples per hour; a single tape will last $\sim$ 3 weeks. Field sites are now "swept" at least once every two weeks and the tapes read using a Datel reader interfaced to a DEC MINC minicomputer. Hexadecimal data are stored on discs and converted to decimal during analysis.

III. DATA

Figures 2 to 5 are representative data sets during the recording periods shown in table 2. We have not observed any activity which might be characterized as "unusual" or related to seismic activity. A small (M = 2.5) earthquake occurred near the Del Sur and Fairmont wells on Day 357 of 1980. However, no pre- or coseismic signals were seen in the Fairmont data (e.g. figure 3); the Del Sur recorder was "down" during this time.

Figure 2 shows hourly averages of water level in the Fairmont well for a one week period in December, 1980. Clearly seen is the response of the well to a combination of the solid earth tides and the S_2 solar diurnal atmospheric tide (Munk and MacDonald, 1966). The atmospheric tide is clearly discernible on barometric records from both Fox Airport near Lancaster and our Bouquet Reservoir strainmeter site. The high frequency ($\sim$ hourly) variation represents the least count "chatter" of the datalogger and is not real. We will be shortly upgrading the resolution to 0.5 mm. Figure 3 shows daily averages of water level in the Fairmont well together with barometric pressure from nearby Fox Airport. The lines on either side of the water level curve represent the 4-sigma band, due, almost exclusively, to the diurnal and semi-diurnal variation. The correlation with barometric pressure is high, with virtually no secular or short term change

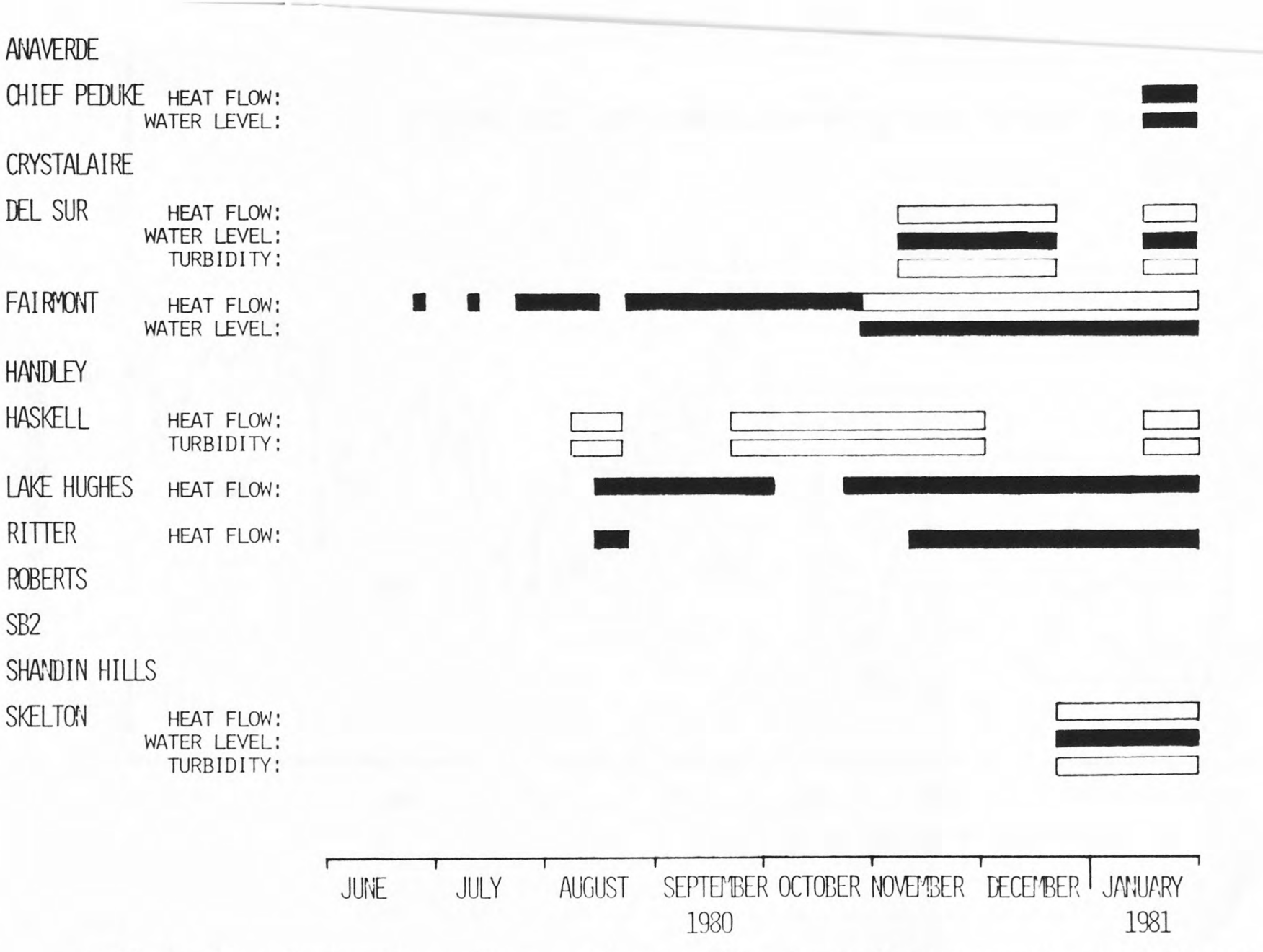

Table 2. Chart showing sites on line as of January, 1981. Darkened bars represent reduced data sets.

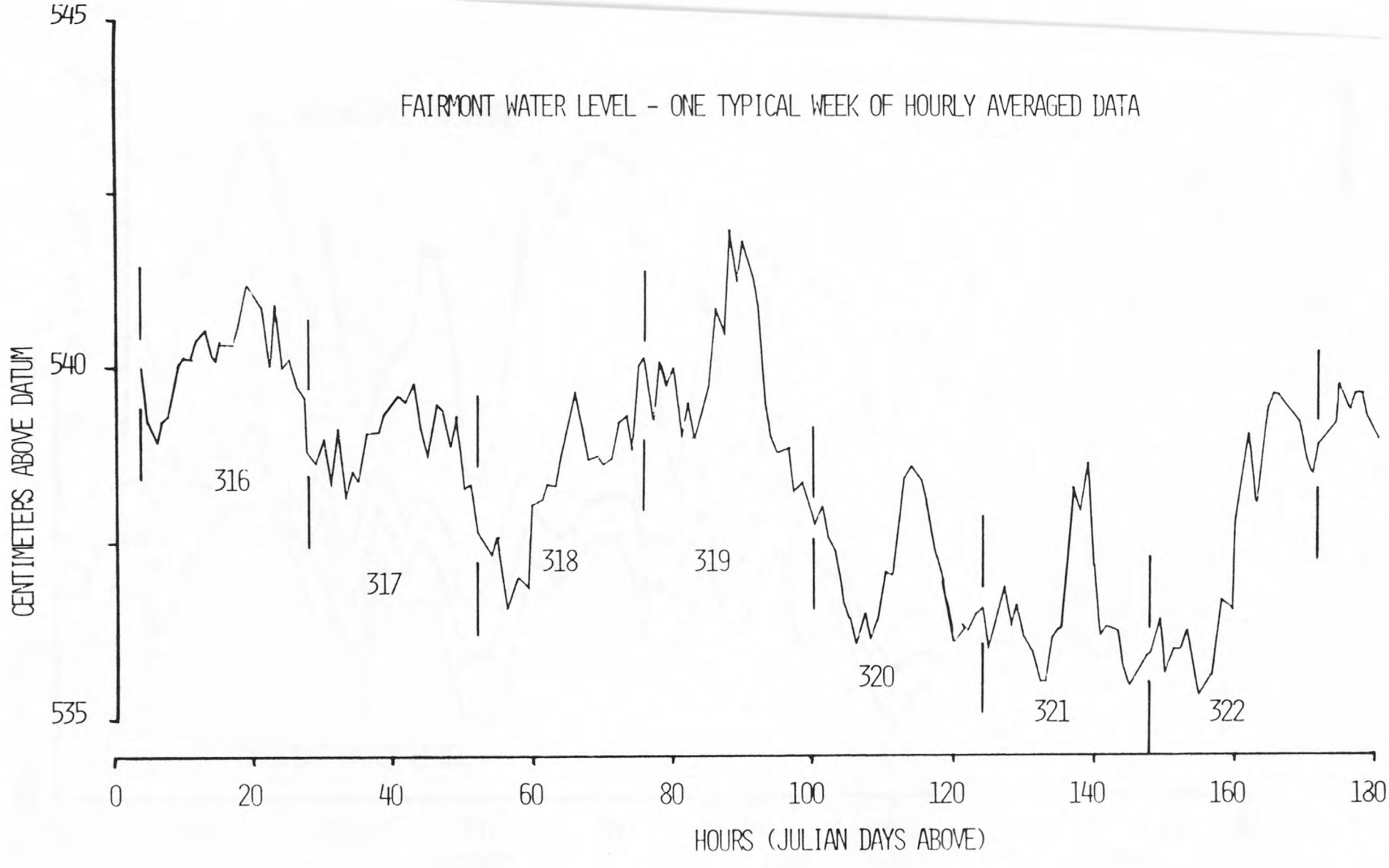
FAIRMONT WATER LEVEL - ONE TYPICAL WEEK OF HOURLY AVERAGED DATA
CENTIMETERS ABOVE DATUM
545
540
535
316
317
318
319
320
321
322
0
20
40
60
80
100
120
140
160
180
HOURS (JULIAN DAYS ABOVE)

FIGURE 2.

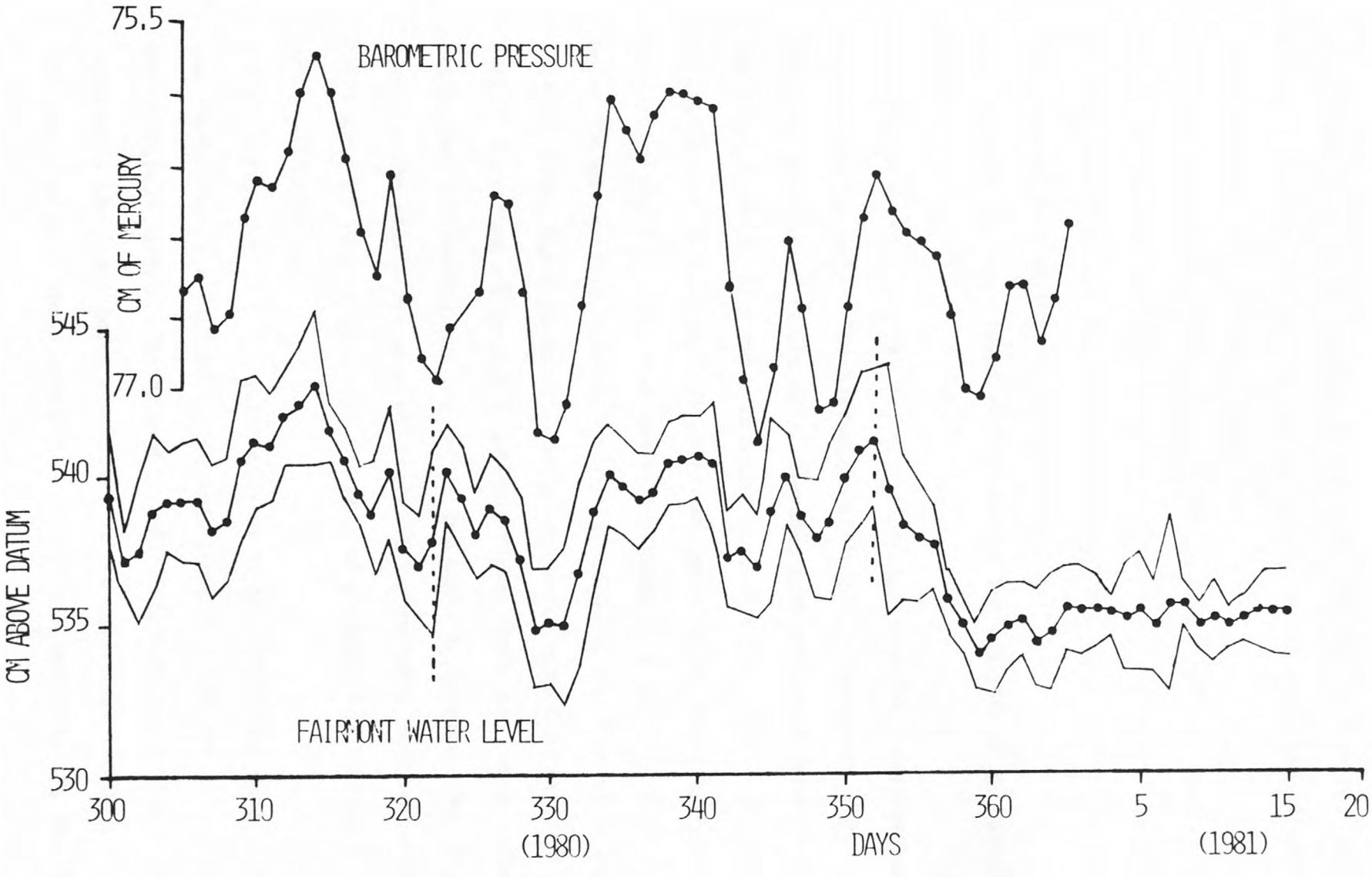
75.5
BAROMETRIC PRESSURE
CM OF MERCURY
77.0
545
540
535
530
CM ABOVE DATUM
FAIRMONT WATER LEVEL
300
310
320
330
340
350
360
5
15
20
(1980)
DAYS
(1981)

FIGURE 3.

in water level seen once the pressure induced level changes are accounted for. Note that the barometric efficiency factor (Jacob, 1940; Bredehoeft, 1967) is on the order of 0.5 for periods on the order of one - two weeks. We plan to monitor this factor with time, and as a function of excitation frequency inasmuch as it reflects bulk aquifer properties.

The equivalent amplification factor (Bredehoeft, 1967) for solid earth tides can, in principal, be treated in the same way. Assuming stationarity or known time dependence of the barometric efficiency and amplification factors, transfer functions between barometric pressure/solid earth tides and water level can be used to generate water level anomaly curves for analysis (e.g. Johnson et al., 1973).

Figure 4 shows similar barometric pressure and daily-averaged water level for the Del Sur well. The barometric efficiency is somewhat higher for this aquifer. Also shown is the daily-averaged turbidity; the decreasing trend during the first 30 days indicates a decrease in turbidity. This is probably the result of settling of particulate matter in the water column after emplacement of the sensors on day 312. The instrument is located at a depth of about 70 meters below the water table. Particles with sizes 0.005 mm (fine silt) and below have settling times for a 70 meter water column which exceed 30 days (Gilluly et al., 1968). Particles are probably sediment fines, rust, etc. which adhere to the casing and are loosened by the cables and water turbulence. Not shown on this plot are the hourly averages which show an appreciable 4-sigma variability. The source of this noise is not yet well understood, but is almost certainly in the electronics.

Finally, figure 5 is representative of the thermistor data. Data from the two thermistors are plotted on two ordinate scales for the post-insertion equilibration period. The apparent variability seen in the lower two curves represents the least count resolution of the datalogger and as such is not real. Thus resolution of these units is $\sim \pm 0.015°C$. Resolution is determined by the

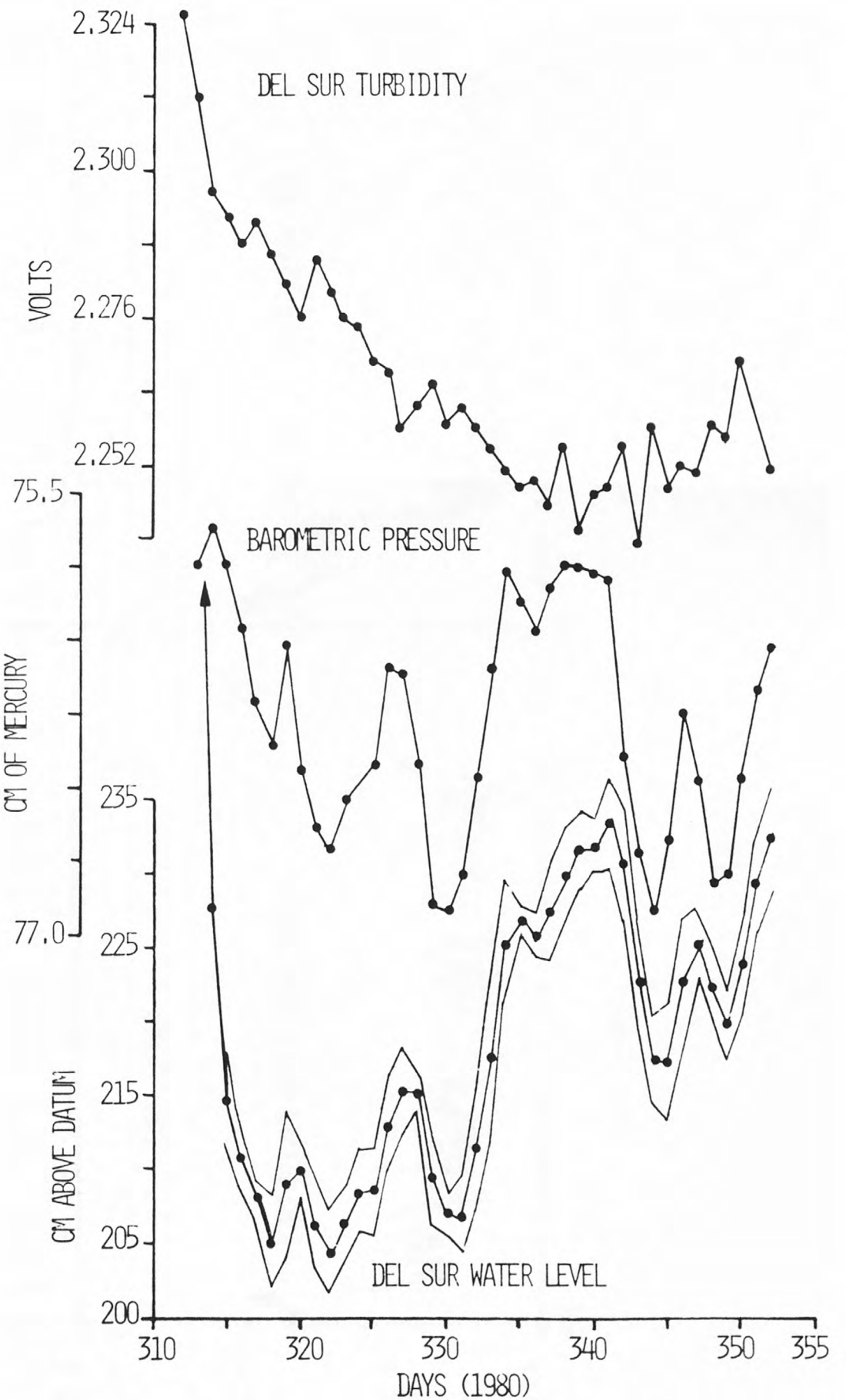
2.324
2.300
2.276
2.252
VOLTS
DEL SUR TURBIDITY
75.5
77.0
CM OF MERCURY
BAROMETRIC PRESSURE
235
225
215
205
200
CM ABOVE DATUM
DEL SUR WATER LEVEL
310
320
330
340
350
355
DAYS (1980)

FIGURE 4.

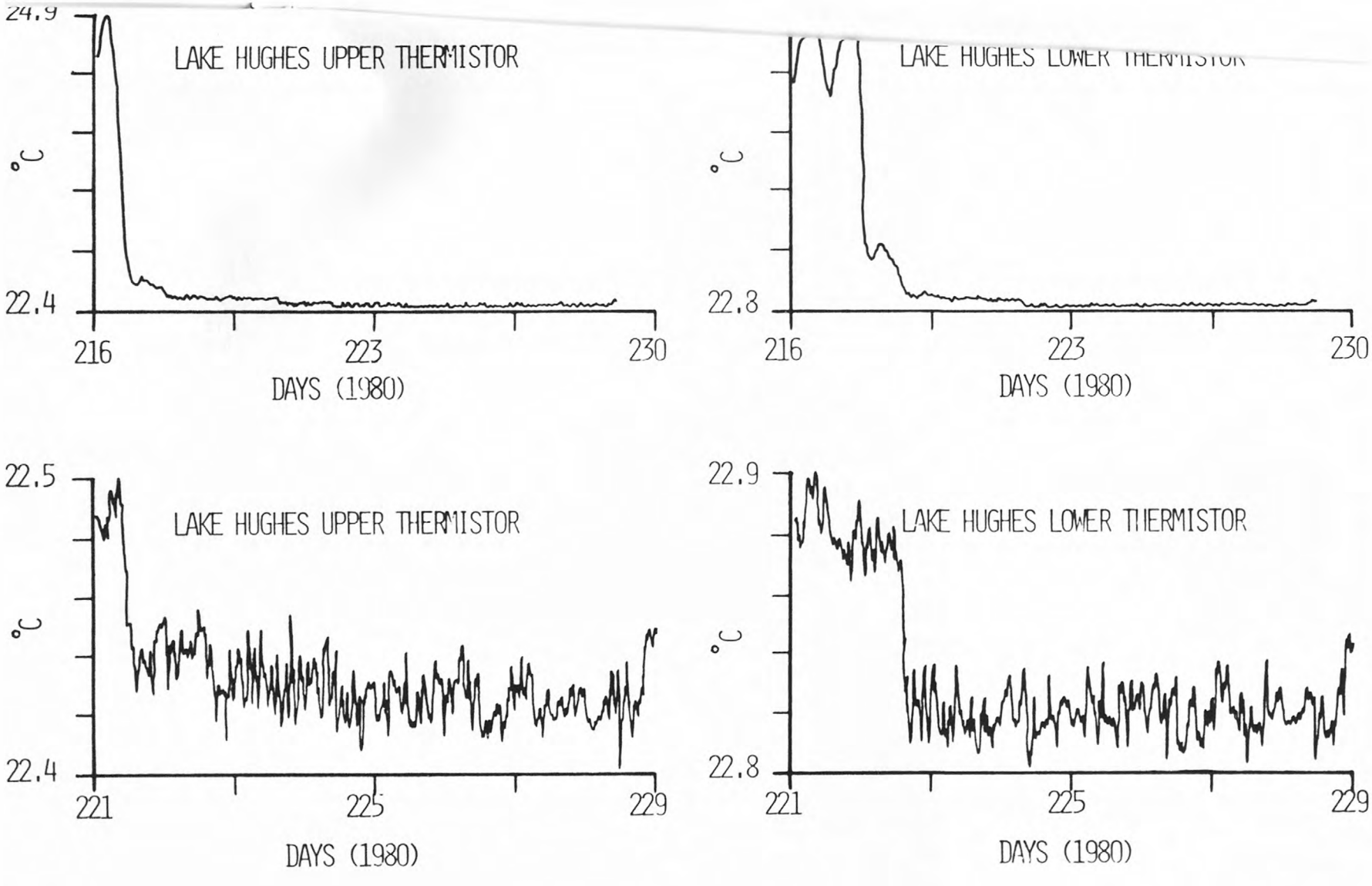
LAKE HUGHES UPPER THERMISTOR
°C
22.4
216
223
230
DAYS (1980)
LAKE HUGHES LOWER THERMISTOR
°C
22.8
216
223
230
DAYS (1980)
22.5
LAKE HUGHES UPPER THERMISTOR
°C
22.4
221
225
229
DAYS (1980)
22.9
LAKE HUGHES LOWER THERMISTOR
°C
22.8
221
225
229
DAYS (1980)

FIGURE 5.

desired range, which in this case is $\sim$ 25°C. For stable holes we plan to reduce the range to $\sim$ 2°C, thereby gaining a resolution $\underset{\sim}{}$ ± 0.001°C.

REFERENCES

Bodvarsson, G., 1970, Confined fluids as strainmeters, Jour. Geophys. Res. 75, p. 2711-2718.

Bredehoeft, J. D., 1967, Response of well-aquifer systems to earth tides, Jour. Geophys. Res. 72, p. 3075-3087.

Gilluly, J., A. C. Waters and A. O. Woodford, 1968, Principles of Geology, W. H. Freeman and Co., San Francisco, 687 pp.

Henyey, T. L., T. L. Teng and D. E. Hammond, 1977, Annual Technical Report, Deepwell monitoring of strain-sensitive parameters over the Southern California Uplift.

Henyey, T. L. et al., 1978, Semi Annual Technical Report, Deepwell monitoring of strain-sensitive parameters over the Southern California Uplift.

Jacob, C. E., 1940, On the flow of water in an elastic artesian aquifer, Trans. Am. Geophys. Un., part 2, p. 574-586.

Johnson, A. G., R. C. Kovach, A. Nur, and J. R. Booker, 1973, Pore pressure changes during creep events on the San Andreas fault, Jour. Geophys. Res. 78, p. 851-857.

Melchior, P., 1956, Sur l'effect des marées terrestes dans les variations de niveau observées dans les puits en particular au sondage de Turnhout (Belgium), Commun. Obs. Roy. Belgique, 108, p. 7-28.

Merrifield, P. M. and D. L. Lamar, 1980, Water level monitoring along San Andreas and San Jacinto faults, southern California, during fiscal year 1980. Technical report 80-2 submitted to U.S.G.S., 77 pp.

Munk, W. H. and G. J. F. MacDonald, 1966, The rotation of the earth, Cambridge University Press, Cambridge, 323 pp.